Benchmarking an automated minirhizotron camera system

by

Jose Guilherme Cesario Pereira Pinto

B.S., Federal University of Santa Catarina, 2018

A THESIS

submitted in partial fulfillment of the requirements for the degree

MASTER OF SCIENCE

Department of Agronomy
College of Agriculture

KANSAS STATE UNIVERSITY
Manhattan, Kansas

2021

Approved by:

Co-Major Professor
Naiqian Zhang

Approved by:

Co-Major Professor
Colby Moorberg

Copyright

Abstract

Understanding plant roots and root development is key for agricultural productivity as roots affect many plant, ecosystem and biogeochemical processes. However, studying root development in-situ can be challenging. Minirhizotrons are commonly used for root monitoring, and allow non-destructive tracking of root development overtime. Nonetheless, existing commercial minirhizotron cameras are expensive and manually operated. Planar optodes are a promising technology for quantifying concentrations of soil solutes, but have not yet been paired with minirhizotron technology. We developed an inexpensive, automated minirhizotron camera system, the RhizoPi camera, built using off-the-shelf computer components that can be paired with planar optodes. The purpose of this study was to evaluate the capability and utility of the RhizoPi camera system. The objectives were to 1) assess the capabilities and design of the RhizoPi minirhizotron camera system and benchmark it against a commercial minirhizotron camera; 2) create an image analysis script to analyze minirhizotron images and compare results to those of existing commercial software; and 3) develop a method for using the RhizoPi camera system for planar optode imaging. Objectives 1 and 2 are the focus of Chapter 2 in which soybean (Glycine max L.) was grown in containers under controlled greenhouse conditions. Images collected using the RhizoPi camera system were analyzed for percentage of images that are roots (root percentage) using a script written in the Python programming language and the RootSnap!® software. Although the average root percentage measured by the Python script, 3.36%, was significantly larger than with RootSnap!, 2.97%, the difference was small in magnitude (0.39%). Images collected using the RhizoPi camera were compared to images collected on the same day using the commercially-available CID Bioscience CI-600 minirhizotron camera. Images from the two camera systems were processed to ensure the exact

image frame location was being compared, then processed using RootSnap!. Objective 3 was the focus of Chapter 3, in which a method is presented for augmenting the RhizoPi minirhizotron camera system with planar oxygen optode technology and techniques. In this method acrylic minirhizotron tubes were turned into oxygen sensitive planar optodes by applying oxygen-sensitive dyes in a strip along the length of each tube. Successful calibrations of these optodes are presented as a proof of concept for this method. The RhizoPi camera system is capable of collecting research-quality images of roots, and can serve as a platform for deploying planar optode technologies for in situ analysis of soil solution chemistry.

Table of Contents

List of Figures vii
List of Tables ix
Acknowledgements x
Dedication xii
Chapter 1 - Literature review 1
Abstract 1
Introduction 1
Growing human population and its demands 1
Importance of plant roots and associated belowground processes 2
Minirhizotron 3
Advantages 4
Disadvantages 4
Developing scientific instruments using Raspberry Pis and other inexpensive computers 7
Python Images Analysis 8
Soil solution chemical measurements (Planar optodes) 9
Summary 13
References 15
Chapter 2 - Benchmarking the RhizoPi automated minirhizotron camera system 22
Abstract 22
Introduction 23
Material and Methods 24
Greenhouse experiment 24
Field experiment 26
Statistical analysis 28
Results 29
Minirhizotron camera comparisons 29
Minirhizotron Camera System Comparisons 30
Image analysis software comparisons 30
Grain yield 31

Discussion 31
Conclusion 34
References 36
Figures and Tables 38
Appendix 60
Chapter 3 - Minirhizotron based planar optodes 69
Abstract 69
Introduction 70
Material and methods 71
Creating Planar Oxygen Optodes with Minirhizotron Tubes 72
Modification of the RhizoPi Minirhizotron Camera System for Imaging Planar Optodes 73
Imaging procedures 73
Calibrating the images 73
Results 76
Sensor calibration 76
Discussion and Conclusion 76
References 78
Figures and Tables 80
Appendix 86

List of Figures

Figure 2.1. Minirhizotron tube with stripe dots to ensure the exact image frame location was being compared. 38
Figure 2.2. Installed minirhizotron with a 60° angle. 39
Figure 2.3. Field operation of the RhizoPi camera system. 40
Figure 2.4. Estimated value for RhizoPi and RootSnap! regression. 41
Figure 2.5. Comparing camera to camera (CI-600 x RhizoPi) using RootSnap! software. 42
Figure 2.6. Camera comparisons. CI-600 (left) and the RhizoPi (right). 43
Figure 2.7. Comparing camera to camera (CI-600 x RhizoPi) using RootSnap! software for different days after emergence (56 and 61). 44
Figure 2.8. Comparing camera to camera (CI-600 x RhizoPi) using RootSnap! software for different depths (0-50 cm and 50-100 cm). 45
Figure 2.9. Comparing system to system (RhizoPi/Python script x CI-600/RootSnap!). 46
Figure 2.10. Software comparisons with RootSnap! (left) and Python script (right) images for the corn roots. The values of root percentage estimations were A- 14.31% and B-17.48%; C-17.8% and D-19.02%; E- 17.8% and F-19.02%. 47
Figure 2.11. Comparing system to system (RhizoPi/Python script x CI-600/RootSnap!) for different days after emergence (56 and 61). 48
Figure 2.12. Comparing system to system (RhizoPi/Python script x CI-600/RootSnap!) for different depths (0-50 cm and 50-100 cm). 49
Figure 2.13. Comparing software to software (Python script x RootSnap!) for RhizoPi images. 50
Figure 2.14. Distribution of camera software by days after emergence (DAE). 51
Figure 2.15. Comparison of two software (Python script x RootSnap!) for the RhizoPi images within depths. 52
Figure 3.1. Tubes and airbrush into the fume hood for coupling the planar optode. 80
Figure 3.2. Coding color after painting. 81
Figure 3.3. Optode calibration tank system. 82
Figure 3.4. An example oxygen optode calibration curve. Dots are mean pixel values for an area of 3 cm^2. This curve is from position 2 of the calibrated optode. 83

Figure 3.5. Pixel intensity of the Red and Green image at different oxygen concentrations for position 2..... 84

List of Tables

Table 2.1. Camera comparison (CI-600 vs. RhizoPi) using RootSnap! software analysis of soybean root images from all dates and depths. 53
Table 2.2. System comparison (RhizoPi/Python script vs. CI-600/RootSnap!) of soybean root images from all dates and depths. 54
Table 2.3. Paired comparison of image measurements. 55
Table 2.4. Comparison of two softwares (Python script x RootSnap!) for the RhizoPi images within days after emergence. 56
Table 2.5. Comparison of two softwares (Python script x RootSnap!) for the RhizoPi images within depths. 57
Table 2.6. Description of agreement analysis between camera software. 58
Table 2.7. Camera's Feature and Specifications for CI-600 and RhizoPi hardwares. 59
Table 3.1. Oxygen rates, red, green and pixel intensity values for optode calibration of position 2. 85

Acknowledgements

I would like to express my sincere gratitude to my advisor Dr. Colby Moorberg. Thank you for your guidance throughout my M.S. program. I appreciate your trust and instruction for both personal and professional matters. I am also grateful to the NSF for providing financial support for my graduate assistantship at Kansas State University, as well as the support from the Kansas EPSCoR MAPS First Awards program, the Kansas Water Resources Initiative, and the Kansas Corn Commission. To my co-advisor, Dr. Niaqian Zhang and committee member, Dr. Kraig Roozeboom, thank you for the mentorship throughout my graduate studies. I greatly appreciated your participation in my project.

To my fellow graduate students and colleagues; Jake Ziggafoos, Mosaed Majrashi, Ben Hamil, Vicki Song, Logan Simon, Brent Jaenisch, Nicolas Giordano, Sevendeep Kaur and Manjot Rekhi. To the intern Cadie Elder for all the help with laboratory work.

This study would not be completed without support from my family and friends. Therefore, I would like to thank the Brazilian community of Manhattan, including but not limited to Lucas Munaro, Andre Fogaça, Ludmilla Monteiro, Gabriel Blair, Raphael Saraiva, Joao Zancanaro, Joao Amaral, Leonardo Miraldo, Giovana Cruppe, among many others who at some point in time made this journey more pleasant. To my friends and mentors Andre Reis, Vinicius Perin, Romulo Lollato, and Amanda Silva for all the support and friendship. I would like to thank, Tony and Barbie, who I consider my family in the US for all the love and friendship. I also extend a very special thanks to my mother Leila Cesario, my father Jose Roberto Pinto, Pinto, my sister Luisa Cesario, my brother Jose Octavio Cesario and my nephew, Leonardo Pinto, my second mother Roseli Aparecida and her family, who provided love and support at a distance, which were fundamental to keep me moving forward throughout such a challenging

path. I am extremely grateful to Roberta Bianchin Rebesquini, for bearing the challenges by my side and for being the best companionship I could have asked for.

Dedication

I dedicate this thesis for my parents, my brother and my sister who always encouraged me to pursue my dreams. Thank you for the endless love and for teaching me compassion and determination.

Chapter 1 - Literature review

Abstract

The global population has quadrupled over the last century. This growth, along with rising incomes, increases global food demand. Understanding root development is vital for sustaining and increasing agricultural productivity due to the influence of roots on many ecosystem and biogeochemical processes. Root research has been inhibited by limitations; most notably high labor requirements and high costs of current root imaging equipment and. A summary of literature related to the use of minirhizotrons for in situ imaging roots and planar optodes for in situ sensing of soil solution chemistry is presented below. Topics reviewed include the advantages and disadvantages of minirhizotrons for studying roots, existing commercial minirhizotron cameras, development of scientific instruments using Raspberry Pi computers and other of-the-shelf computer components, use of the Python programming language for image analysis, and the use of planar optode sensors for two-dimensional quantification of soil solution chemistry. Understanding this environment is critical. Thus, minirhizotron cameras that are inexpensive, fully automated, and complimented by rapid image analysis and soil solution chemistry sensing with planar optodes are a promising advancement in the study of soil, root, and rhizosphere science.

Introduction

Growing human population and its demands

Global demands for food and feed are increasing, which stresses land, water, nutrient, and soil resources (Eshel and Beeckman, 2013). Plant root systems serve as the nexus between these vital resources (Wang et al., 2006). Therefore, there is a need to develop our fundamental

understanding of root growth and development, and the impact of the presence of roots on the belowground environment. A cost-effective automated minirhizotron camera system combined with open-source data analysis to monitor rooting dynamics represents a big step towards supporting research to meet the demands of our land, water, nutrient, and soil resources. In this chapter I will review the importance of roots, methods of analyzing roots, and inexpensive computer tools for root analysis, such as the Raspberry Pi and Python image analysis.

Importance of plant roots and associated belowground processes

Although most studies on plant growth have focused on aboveground organisms (Balvanera et al., 2006), plant roots and related belowground processes are essential for agricultural production and, similarly, for local and global water, carbon and nutrient cycles (Eshel and Beeckman, 2013; Kirkham, 2014).

Although it is clearly important, research on roots has been inhibited by constraints imposed by the limitations of technology and the relatively labor-intensive nature of root research using existing technologies and methodologies (Persson, 1990). Environmental conditions can change through space and time (Polomski and Kuhn, 2002). Thus, temporal patterns of root distribution are commonly estimated in the field using repeated sampling, often in the form of consecutive soil core sampling (Crossley Jr and Blair, 1991; Rusek, 2001). The main issue related to soil core sampling for belowground variables is that spatial variability is often combined with temporal sampling. Cores from slightly different locations are inspected each day. (Johnson et al., 2001; Smith and Read, 2009). This can be avoided by using minirhizotrons, which gather images of soil biota with minimal disruption (Steinaker and Wilson, 2008).

According to Mancuso (2011), root research has advanced greatly in recent years because of significant advances in root imaging technology and methodology. However, most approaches have focused on container studies, growth of plants on non-soil media, or genetically modified root plants that brighten to grant greater root-soil contrast to promote automated image analysis. Limitations, such as small container size and unnatural soil properties or growing conditions, exist with each of these methods (French et al., 2012). A key challenge for belowground investigations is non-destructively collecting data at spatial and temporal scales that are relevant to the studied processes. The merger of belowground imaging and two-dimensional soil sensing can address this challenge through the use of minirhizotrons.

Minirhizotron

Minirhizotrons have been used for more than 80 years going back to Bates (1937), and are viewed as a low-cost alternative to large, underground rhizotrons (Böhm, 1979). Rhizotrons normally comprise of an underground cellar or walkway with walls or windows that come into direct contact with the natural soil profile (Taylor et al., 1990a). In contrast, minirhizotrons are transparent tubes inserted into the soil to permit repeated root observation (Taylor et al., 1990a; Gregory, 2006). As the quality of cameras and associated electronics improved, the importance of minirhizotrons for studying root dynamics has increased in agronomy, forestry, and other soil and plant science disciplines (Hendrick and Pregitzer, 1996). Minirhizotrons have distinct advantages over conventional rhizotrons as well as other methods of studying roots *in situ*. However, the technology is not without disadvantages.

Advantages

The primary advantage of using minirhizotrons is that roots can be non-destructively studied *in situ* (Ephrath et al., 1999). Most other study methods are destructive and demand separation of the roots from the soil, generally by washing (Böhm, 1979). Also, minirhizotrons are versatile – they can be introduced in a wide diversity of ecological conditions (Gregory, 2006; Wilson, 2014). Additionally, minirhizotron camera systems that are inserted into the minirhizotron tubes facilitate taking sequential root images over extended time periods (Hendrick and Pregitzer, 1996; Majdi, 1996). These images can then be analyzed to provide quantitative data on root length, mortality, longevity, density, diameter, and architecture (Hendrick and Pregitzer, 1996). Moreover, minirhizotrons have the capacity to track specific roots from the beginning until senescing without interfering significantly on the fine root mechanism (Johnson et al., 2001a). Various commercial and open-source software has been developed to facilitate collection and analysis of these images, including RootSnap!™ (CID Bio-Science, Camas, WA, USA) WinRHIZO™ (Regent Instruments Inc., Ottawa, ON Canada), and RootFly 2.0.2 (Zeng et al., 2008).

Disadvantages

Although minirhizotrons provide clear advantages over other methods of studying roots, there are disadvantages. First, root length data cannot be directly converted into dry mass. Therefore, soil cores are necessary to estimate biomass production (Böhm, 1979). Minirhizotron-based experiments also can be costly, especially with regard to labor and camera costs (Jose et al., 2001). Minirhizotron installation plays a critical role in the quality of resulting data due to the contact between the soil and the minirhizotron tube. If tube insertion causes compaction it may result in artificially low root counts. Conversely, if a gap occurs between the tube and soil due to

an over-sized auger hole size, it may result in artificially high root counts as roots follow a path of least resistance in the soil along the viewing surface of the tube (Brown and Upchurch, 1987; Johnson et al., 2001b).

A significant factor that limits the minirhizotron method is the considerable amount of labor necessary for collecting and analyzing root images (Persson, 1990; Zeng et al., 2008; Vamerali et al., 2012a). Currently, commercially available minirhizotron cameras are all manually operated and require a researcher to regularly visit field sites to collect images. Furthermore, the amount of labor required to analyze root images can be several times the amount of labor required to collect the images (Svane et al., 2019). Thus, the requirement for manual image collection and analysis limits the number of minirhizotron tubes that can be installed in a given experiment, limiting number of treatments and replications. A few minirhizotron prototypes, such as AMR-A (RhizoSystems LLC) and SoilCam (Rahman et al., 2020), have showcased advanced features that automate the counting. However, these features have not been adopted by the market, likely because of limitations from image blur, distortion, and coloration (using mirrors due to narrow MR tubes), and low positioning accuracy (Rewald et al., 2020).

Despite different endeavors made within the last decade, root image analysis is still based on manual root tracing. There have been several automated root tracing techniques and algorithms developed for analyzing minirhizotron root images, including Rootfly (Zeng et al., 2008), RootSnap! (Version 1.3.2.23, CID-Bioscience, Camas, WA, USA), etc. However, the utility of these algorithms is limited by low contrast between soil and roots. (Svane et al., 2019). Moreover, uneven illumination generated by the light sources, soil property changes, and artifacts (scratches, water condensation, etc.) make computerized minirhizotron image

examination challenging (Rewald et al., 2020). Lastly, root imaging using minirhizotrons provides information only about rooting dynamics. Soil properties must be quantified separately from root images. Thus, there is a disconnect in space and time between minirhizotron-imaged root data and soil chemical, physical, and biological properties. Although root imaging with minirhizotron technologies have advanced knowledge of ecology, plant ecophysiology, and soil fertility (Johnson et al., 2001b; Vamerali et al., 2012b; Iversen et al., 2012), these technologies alone do not provide further insight into belowground biogeochemical environment.

Available minirhizotron cameras

There are three companies that manufacture minirhizotron cameras at present: i) CID-BioScience Inc., Camas, WA, USA, ii) RhizoSystems LLC, Idyllwild, CA, USA, and iii) Vienna Scientific Instruments & Bartz Technology Corporation. Roberti et al. (2014) compared the CI-600 In-Situ Root Imager (CID-BioScience) with the automated minirhizotron version A (AMR-A; RhizoSystems LLC). They used a laboratory approach to compare the primary operations of these minirhizotron cameras and evaluated correlated uncertainties. Unlike the CI-600, which is manually controlled and works on a scanner-based digital technology and an open system, the AMR-A is entirely automated, programmable equipment that operates a digital microscopic camera in a closed system.

Both minirhizotron cameras presented advantages and limitations built in their hardware and operation management. For the CI-600, human errors occurred when the manual minirhizotron camera was removed and replaced. In contrast, the AMR-A presented unexpected heating due to soil conditions, which depended on the number of repetitions in imagery taking. The above mentioned factors should be considered when analyzing minirhizotron images so that

the technologies can be improved and a better understanding of the belowground processes can be achieved (Roberti et al., 2014).

Using information and communication technology (ICT) to develop and process farming information is essential to rural production, management, and operations (Li, 2009).
The essence of agriculture informatization is to digitize each process in agriculture (animal husbandry, crop production, aquaculture, and forestry) through data innovation. Agriculture technology increased in sophistication with advances in modern technology, in particular with the advent of broad connectivity and the Internet of Things (IoT) (Yan-e, 2011).

Developing scientific instruments using Raspberry Pis and other inexpensive computers

Internet of Things (IoT) is the interconnection of extraordinarily identifiable gadgets to provide remote monitoring or control assistance (He et al., 2017). The IoT is very prevalent in many areas, one example being home automation. The use of single-board computers and open-source software has allowed do-it-yourself-minded individuals to create their own IOT devices inexpensively. (Sruthy and George, 2017). Inexpensive Raspberry Pi computers (Raspberry Pi Foundation) and free, open-source software have helped facilitate this IoT creativity (Gonzalez et al., 2016).

Raspberry Pi computers are small boards, approximately 8.5 by 5.3 cm. These single board computers were initially planned to help to advance coding abilities (Upton and Halfacree, 2012). Most contemporary models highlight built-in modules for wireless and
Bluetooth networks (Monk, 2016). Furthermore, the Raspberry Pi Foundation (Cambridge, United Kingdom) issues open-source software and accomplices such as camera modules. Supplementary sensors or controllers can be attached through USB ports and general-purpose input/output pins. Raspberry Pis can operate parallel tasking and information approaches in real-

time (Alvarez-Rosario and Padovese, 2015). Due to its low price and great capabilities, Raspberry Pi computers have gained great popularity for scientific applications (Tovar et al., 2018), including data collection and monitoring systems for agricultural applications, such as plant care and selective irrigation to enhance the productivity and efficacy of water management (Grindstaff et al., 2019). Raspberry Pis have also been used as part of automated minirhizotrons systems for the AMR camera and SoilCam (Rewald et al., 2020; Rahman et al., 2020). In both cases, the cameras are fully automated and an image-processing software was developed to enable estimations of root growth patterns.

Alongside advances made for automating image collection for minirhizotrons, similar advances have been made in image analysis automation. They have been broadly embraced for fast and useful root phenotyping. These technologies have been made accessible through commercial software applications (Cai et al., 2015), such as WinRHIZO^{TM} and the open-source software options such as SmartRoot (Lobet et al., 2011), RootTrace (Clark et al., 2011), EZ-Rhizo (Armengaud et al., 2009), Root System Analyzer (Leitner et al., 2014), IJ_Rhizo (Pierret et al., 2013), RootNav (Pound et al., 2013), and CRootBox (Schnepf et al., 2018). These software solutions, either semi- or fully-automated, were used to investigate roots shown in high-quality 2D scans (Cai et al., 2015). Some machine learning algorithms were implemented using various software packages, such as R, MATLAB, and Python. However, there has been limited success in automated minirhizotron image analysis (Zhu et al., 2010; Vicensi et al., 2020).

Python Images Analysis

An open-source programming language that is frequently used with Raspberry Pi computers is Python (Sanner, 1999). Python is an explained, interactive, object-oriented programming language. It presents high-profile data frameworks, such as list and associative

arrays called dictionaries, compelling typing and binding, modules, classes, exceptions, and automated memory administration. It has an exceptionally clean and refined syntax and still is a potent and general-purpose programming language (Sanner, 1999).

Python supports image analysis through the use of toolkits such as Scikit (Pedregosa et al., 2011). Scikit is an open-source image processing toolkit that supports an extensive number of file formats, and is suitable with two- and three-dimensional images. The toolkit uses a simple programming interface with thematic modules organizing functions according to their aims, such as image restoration, apportionment, and analysis. (Gouillart et al., 2016).

The capacity to gather quality information in a short time or truly redeem high-resolution pictures from under-sampled, blurred, and disturbed data can practically enhance experimental outcomes, possibly leading to novel disclosures (Farrens et al., 2020). These functions for image analysis also can be applied to planar optodes.

Python pairs well with Raspberry Pi due to its low cost, proficiency in hardware control, and analytical capabilities (Sanner, 1999). This makes Python an ideal language for use on a Raspberry Pi-based, automated minirhizotron camera system, as it would facilitate both image collection and analysis (Rahman et al., 2020). In addition, with the correct hardware accessories, Raspberry Pi computers and Python can be used in a minirhizotron camera platform to facilitate *in situ* soil solution chemical measurements with planar optode sensors (Faget et al., 2013).

Soil solution chemical measurements (Planar optodes)

According to Darrah (1993) the rhizosphere is described as the soil volume around living plant roots influenced by root activity. Understanding this environment is critical, mainly when it comes to the biological process analysis (Hinsinger et al., 2005). Therefore, analyzing factors such as soil bulk density interactions, spatial and temporal dynamics of O_2, pH, and CO_2 is vital

to comprehend plant roots (Blossfeld et al., 2013b). The standard measuring technique for sensing dissolved O_2 and CO_2 are (micro-) electrodes. However, electrodes are based on the electrochemical principle during the evaluation, which requires the electrode to be inserted into the biological environment. Thus, the method is invasive and can be disadvantageous for the assessment of sensitive bioprocesses. Electrodes have proven to provide excellent quantitative data on O_2 and CO_2 concentration or pH rates under lab and field conditions (Revsbech et al., 1999; Armstrong, 2000). However, quantitative mapping of these analytes would demand a large set of fixed microelectrodes, each covering less than a square millimeter of the analyzed space of the growing roots (Fischer et al., 1989). Besides, quantitative data of radial and axial profiles of living roots with microelectrodes can only be derived when functioning under artificial conditions (Taylor and Bloom, 1998; Bloom et al., 2003). Therefore, non-invasive techniques for accurate high-resolution investigations of soil bioprocesses are required.

Optodes are an emerging technology that overcomes the drawbacks of established sensors and technologies to quantify environmental parameters, such as ion-selective electrode (ISE). In addition, optodes could be paired with minirhizotron technologies (Blossfeld and Gansert, 2012). The measurement principle of oxygen optodes is based on the dynamic quenching of a fluorescent indicator through oxygen (Kautsky, 1939). The fluorophore is a fluorescent chemical compound that can re-emit light upon excitation. It consumes light within the nonappearance of oxygen and transmits the consumed energy as fluorescence with a determined intensity and period (Klimant et al., 1995; Hartmann and Ziegler, 1996). For planar sensing, the fluorescent indicator is immobilized on thinned transparent foils. The intensity and lifetime distribution on the foil of oxygen-sensitive fluorescence are computed by a digital camera system (Glud et al., 1996; Liebsch et al., 2000). Therefore the planar optodes settle some

of the limitations of describing oxygen disposal at heterogeneous, three-dimensional interfaces with one-dimensional microprofiles (Buffle and Horvai, 2000). The optodes generally appear as planar designs, or are applied to ends of fiber optic cables. Both methods are efficient but selection of the method is based on the spatial requirements of the analysis. For example, the planar methods facilitate evaluations of larger surface areas and can be used in tank set-ups (e. g. Glud et al., 1996; Precht et al., 2004). On the other hand, the fiber design is adapted for observing smaller surface areas and in-situ samples in various fields from medicine (Chen et al., 2013) to environmental research for instance (Klimant et al., 1997).

Planar optodes are non-invasive sensors that rely on imaging of fluorescent dyes that react to changes in soil solution chemistry. Examples of parameter and analytes that can be measured are pH (Blossfeld et al., 2013), dissolved oxygen (Larsen et al., 2011b), and carbon dioxide (Blossfeld et al., 2013). Planar optode measurements offer an unique opportunity to resolve both spatial and temporal variations on a submillimeter scale for a range of analytes (Larsen et al., 2011b). This strategy has previously been utilized to study oxygen dynamics across various benthic water interfaces, (Precht et al., 2004; Wenzhöfer and Glud, 2004) and, very recently, the capability of planar optodes for rhizosphere studies have been presented (Jensen et al., 2005).

In many areas of the world, soil acidity limits agricultural yield. The low content of base cations, especially calcium and aluminum toxicities affect root growth and the absorption of water and nutrients by plants, usually causing a reduction in crop yields on acid soils (Marsh and Grove, 1992; Sumner, 1995; Tang et al., 2003). Thus, optodes speak for a promising technology for estimating soil solution chemical concentrations *in situ*, that has a potential for creating practices to solve these field problems in the future. The innovation consists of dyes embedded in

plastic that are sensitive to oxygen, acidity, carbon dioxide, and other dissolved substances (Blossfeld and Gansert, 2012). The dyes, when energized with light at dye-specific wavelengths, fluoresce at intensities that vary with the target analyte concentration. The ratio of the intensity of fluourescence across different colors can be used to calibrate these optodes and determine analyte concentration at different points. Early studies adopting the colorratiometric method were established on a single-CCD camera that splits the emission light into three primary colors: red, green, and blue (Jiang et al., 2017).

Calibrated planar optodes enable repeatable, two-dimensional estimation of analyte concentrations at millimeter resolution (Blossfeld and Gansert, 2012). Planar optodes are promising and beneficial for a better understanding of the soil biological processes. On the other hand, it has its limitations too. In general, the temporal resolution is not a limitation because the fluorescence responseof the planar optode occurs within μs of excitation of the dye by the light source. However, this requires a transparent pathway for the light to reach the planar optode dye, and for light from fluorescence to be transmitted to the light sensor measuring the fluorescence (Blossfeld, 2013). Rhizoboxes have been used to solve this problem in laboratory settings, but it is challenging in the field.

Early applications of optical procedures under field conditions have been used to collect point data or one-dimensional array data under field conditions with the utilization of optical sensors installed on the ends of fiber optic cables (Rickelt et al., 2013; Larsen et al., 2016). However, such an approach is limited in the spatial detail provided to only point data along a depth gradient.

An advancement on that approach is to arrange point data in a grid to collect data in two dimensions. Schreiber et al. (2012) used this approach by arranging the fiber optic ends in a grid

of measurement spots 1.5 mm apart horizontally and vertically. Then the discrete data from each fiber was interpolated to achieve a quantitative image. Planar optodes, however, allow two-dimensional sensing of soil chemistry and, hence, produce a progressively complete picture of biogeochemical processes.

There are limitations to planar optodes though. Planar optodes do not directly acquire original analyte concentration data, but rather the response of the planar optode dye fluorescence to analyte concentration (Larsen et al., 2011). Further, the dyes are not transparent to allow inspection of roots and other objects, and the soil adjacent to the optode may further obscure roots in close vicinity to the optode (Fischer et al., 1989). As a result, the planar optode can potentially present a shift of analyte values without an evident root behind the optode. Also, calibration issues related to the determination of the indicator concentration have regularly inhibited the use of these methods (Caldwell et al., 1992). Another factor to consider is that all optical sensors are sensitive to temperature, and the measurements should be compensated in case temperature is not kept constant (Borisov et al., 2011). In addition, planar optodes require cameras to image the fluorescence. This requires separation of the camera from the planar optode, which limits how compact planar optode imaging sysems can be. Lastly, it is essential to shield the system from other interfering light sources since the light is the information carrier (Blossfeld, 2013).

Summary

Over the last century the global population has quadrupled. This growth, along with rising incomes, is driving up global food demand. This demand will require agriculture to enhance productivity through new technologies. Because roots are essential for plant functions,

such as water absorption, nutrient uptake, and anchorage, they can directly affect agricultural production. Thus, understanding soil-root interactions remains a topic that needs further exploration in order to meet this increased food demand. Non-destructive root study methods, such as minirhizotrons, are fundamental for facilitating this exploration. Moreover, coupling this method with planar optodes for oxygen rate measurements would be a novel approach to understand soil biological processes. These methods have their limitations, such as the need for collecting data at various spatial and temporal scales and the demand for intensive labor. Thus, automating the measurements would have a significant impact on research. A fully automated system can be built on Raspberry Pis to enable the camera functionalities while using Python programming for image analysis. In summary, this method can help to elucidate the belowground biogeochemical environment.

References

Alvarez-Rosario, A., and L.R. Padovese. 2015. Real-time performance of energy based underwater acoustic event detectors embedded in a single-board computer. 2015 IEEE/OES Acoustics in Underwater Geosciences Symposium (RIO Acoustics). IEEE, Rio de Janeiro, Brazil. p. 1–5

Armengaud, P., K. Zambaux, A. Hills, R. Sulpice, R.J. Pattison, et al. 2009. EZ-Rhizo: integrated software for the fast and accurate measurement of root system architecture. Plant J. 57(5): 945–956. doi: 10.1111/j.1365-313X.2008.03739.x.

Armstrong, W. 2000. Oxygen distribution in wetland plant roots and permeability barriers to gas-exchange with the rhizosphere: a microelectrode and modelling study with Phragmites australis. Ann. Bot. 86(3): 687–703. doi: 10.1006/anbo.2000.1236.

Balvanera, P., A.B. Pfisterer, N. Buchmann, J.-S. He, T. Nakashizuka, et al. 2006. Quantifying the evidence for biodiversity effects on ecosystem functioning and services: Biodiversity and ecosystem functioning/services. Ecol. Lett. 9(10): 1146–1156. doi: 10.1111/j.1461-0248.2006.00963.x.

Bates, G. 1937. A device for the observation of root growth in the soil. Nature 139(3527): 966.

Bloom, A.J., P.A. Meyerhoff, A.R. Taylor, and T.L. Rost. 2003. Root development and absorption of ammonium and nitrate from the rhizosphere. J. Plant Growth Regul. 21(4): 416–431. doi: 10.1007/s00344-003-0009-8.

Blossfeld, S. 2013. Light for the dark side of plant life: —Planar optodes visualizing rhizosphere processes. Plant Soil 369(1–2): 29–32. doi: 10.1007/s11104-013-1767-0.

Blossfeld, S., and D. Gansert. 2012. The Use of Planar Optodes in Root Studies for Quantitative Imaging. Measuring Roots. Springer, Berlin, Heidelberg. p. 83–92

Blossfeld, S., C.M. Schreiber, G. Liebsch, A.J. Kuhn, and P. Hinsinger. 2013a. Quantitative imaging of rhizosphere pH and CO2 dynamics with planar optodes. Ann. Bot. 112(2): 267–276.

Blossfeld, S., C.M. Schreiber, G. Liebsch, A.J. Kuhn, and P. Hinsinger. 2013b. Quantitative imaging of rhizosphere pH and CO2 dynamics with planar optodes. Ann. Bot. 112(2): 267–276. doi: 10.1093/aob/mct047.

Böhm, W. 1979. Methods of studying root systems. Springer Science & Business Media.

Borisov, S.M., R. Seifner, and I. Klimant. 2011. A novel planar optical sensor for simultaneous monitoring of oxygen, carbon dioxide, pH and temperature. Anal. Bioanal. Chem. 400(8): 2463–2474. doi: 10.1007/s00216-010-4617-4.

Brown, D.A., and D.R. Upchurch. 1987. Minirhizotrons: a summary of methods and instruments in current use. In: Taylor, H.M., editor, ASA Special Publications. American Society of

Agronomy, Crop Science Society of America, Soil Science Society of America, Madison, WI, USA. p. 15–30

Cai, J., Z. Zeng, J.N. Connor, C.Y. Huang, V. Melino, et al. 2015. RootGraph: a graphic optimization tool for automated image analysis of plant roots. J. Exp. Bot. 66(21): 6551–6562. doi: 10.1093/jxb/erv359.

Caldwell, D.E., D.R. Korber, and J.R. Lawrence. 1992. Confocal laser microscopy and digital image analysis in microbial ecology. In: Marshall, K.C., editor, Advances in Microbial Ecology. Springer US, Boston, MA. p. 1–67

Chen, R., H. McPeak, F. Formenti, C. Hahn, A. Farmery, et al. 2013. Optimizing sensor design for polymer fibre optic oxygen sensors. 2013 IEEE SENSORS. IEEE, Baltimore, MD, USA. p. 1–4

Clark, R.T., R.B. MacCurdy, J.K. Jung, J.E. Shaff, S.R. McCouch, et al. 2011. Three-dimensional root phenotyping with a novel imaging and software platform. Plant Physiol. 156(2): 455–465. doi: 10.1104/pp.110.169102.

Crossley Jr, D., and J.M. Blair. 1991. A high-efficiency,"low-technology" Tullgren-type extractor for soil microarthropods. Agric. Ecosyst. Environ. 34(1–4): 187–192.

Darrah, P.R. 1993. The rhizosphere and plant nutrition: a quantitative approach. In: Barrow, N.J., editor, Plant Nutrition — from Genetic Engineering to Field Practice. Springer Netherlands, Dordrecht. p. 3–22

Ephrath, J.E., M. Silberbush, and P.R. Berliner. 1999. Calibration of minirhizotron readings against root length density data obtained from soil cores. Plant Soil 209(2): 201–208. doi: 10.1023/A:1004556100253.

Eshel, A., and T. Beeckman. 2013. Plant roots: the hidden half. CRC press.

Faget, M., S. Blossfeld, P. von Gillhaussen, U. Schurr, and V.M. Temperton. 2013. Disentangling who is who during rhizosphere acidification in root interactions: combining fluorescence with optode techniques. Front. Plant Sci. 4: 392. doi: 10.3389/fpls.2013.00392.

Farrens, S., A. Grigis, L. El Gueddari, Z. Ramzi, C. G.R., et al. 2020. PySAP: Python Sparse Data Analysis Package for multidisciplinary image processing. Astron. Comput. 32: 100402. doi: 10.1016/j.ascom.2020.100402.

Fischer, W.R., H. Flessa, and G. Schaller. 1989. pH values and redox potentials in microsites of the rhizosphere. Z. Für Pflanzenernähr. Bodenkd. 152(2): 191–195. doi: 10.1002/jpln.19891520209.

French, A., D. Wells, N. Everitt, and T. Pridmore. 2012. High-throughput quantification of root growth. Measuring Roots. Springer. p. 109–126

Glud, R., N. Ramsing, J. Gundersen, and I. Klimant. 1996. Planar optrodes: a new tool for fine scale measurements of two-dimensional O2 distribution in benthic communities. Mar. Ecol. Prog. Ser. 140: 217–226. doi: 10.3354/meps140217.

Gonzalez, S., T.R. Vargas, P. Arce, and J.C. Guerri. 2016. Energy optimization for video monitoring system in agricultural areas using single board computer nodes and wireless ad hoc networks. 2016 XXI Symposium on Signal Processing, Images and Artificial Vision (STSIVA). IEEE, Bucaramanga, Colombia. p. 1–7

Gouillart, E., J. Nunez-Iglesias, and S. van der Walt. 2016. Analyzing microtomography data with Python and the scikit-image library. Adv. Struct. Chem. Imaging 2(1): 18. doi: 10.1186/s40679-016-0031-0.

Gregory, P.J. 2006. Plant roots: growth, activity, and interaction with soils. Blackwell Pub, Oxford ; Ames, Iowa.

Grindstaff, B., M.E. Mabry, P.D. Blischak, M. Quinn, and J. Chris Pires. 2019. Affordable remote monitoring of plant growth in facilities using Raspberry Pi computers. Appl. Plant Sci. 7(8). doi: 10.1002/aps3.11280.

He, N., R. Bukralia, and H. Huang. 2017. Teaching wireless networking technologies in the internet-of-things using ARM based microcontrollers. 2017 IEEE Frontiers in Education Conference (FIE). IEEE, Indianapolis, IN. p. 1–4

Hendrick, R.L., and K.S. Pregitzer. 1996. Applications of minirhizotrons to understand root function in forests and other natural ecosystems. Plant Soil 185(2): 293–304. doi: 10.1007/BF02257535.

Hinsinger, P., G.R. Gobran, P.J. Gregory, and W.W. Wenzel. 2005. Rhizosphere geometry and heterogeneity arising from root-mediated physical and chemical processes: Research review. New Phytol. 168(2): 293–303. doi: 10.1111/j.1469-8137.2005.01512.x.

Iversen, C.M., M.T. Murphy, M.F. Allen, J. Childs, D.M. Eissenstat, et al. 2012. Advancing the use of minirhizotrons in wetlands. Plant Soil 352(1–2): 23–39. doi: 10.1007/s11104-011-0953-1.

Jensen, S.I., M. Kühl, R.N. Glud, L.B. Jørgensen, and A. Priemé. 2005. Oxic microzones and radial oxygen loss from roots of Zostera marina. Mar. Ecol. Prog. Ser. 293: 49–58.

Jiang, Yu, and Hao. 2017. Design and fabrication of a ratiometric planar optode for simultaneous imaging of ph and oxygen. Sensors 17(6): 1316. doi: 10.3390/s17061316.

Johnson, M.G., D.T. Tingey, D.L. Phillips, and M.J. Storm. 2001a. Advancing fine root research with minirhizotrons. Environ. Exp. Bot. 45(3): 263–289. doi: 10.1016/S0098-8472(01)00077-6.

Johnson, M.G., D.T. Tingey, D.L. Phillips, and M.J. Storm. 2001b. Advancing fine root research with minirhizotrons. Environ. Exp. Bot. 45(3): 263–289. doi: 10.1016/S0098-8472(01)00077-6.

Jose, S., A.R. Gillespie, J.R. Seifert, and P.E. Pope. 2001. Comparison of minirhizotron and soil core methods for quantifying root biomass in a temperate alley cropping system. Agrofor. Syst. 52(2): 161–168. doi: 10.1023/A:1010667921970.

Kirkham, M.B. 2014. Principles of soil and plant water relations. Academic Press.

Klimant, I., M. Kühl, R.N. Glud, and G. Holst. 1997. Optical measurement of oxygen and temperature in microscale: strategies and biological applications. Sens. Actuators B Chem. 38(1–3): 29–37. doi: 10.1016/S0925-4005(97)80168-2.

Larsen, M., S.M. Borisov, B. Grunwald, I. Klimant, and R.N. Glud. 2011a. A simple and inexpensive high resolution color ratiometric planar optode imaging approach: application to oxygen and pH sensing. Limnol. Oceanogr. Methods 9(9): 348–360.

Larsen, M., S.M. Borisov, B. Grunwald, I. Klimant, and R.N. Glud. 2011b. A simple and inexpensive high resolution color ratiometric planar optode imaging approach: application to oxygen and pH sensing. Limnol. Oceanogr. Methods 9(9): 348–360. doi: 10.4319/lom.2011.9.348.

Larsen, M., P. Lehner, S.M. Borisov, I. Klimant, J.P. Fischer, et al. 2016. In situ quantification of ultra-low O2 concentrations in oxygen minimum zones: Application of novel optodes. Limnol. Oceanogr. Methods 14(12): 784–800. doi: 10.1002/lom3.10126.

Leitner, D., B. Felderer, P. Vontobel, and A. Schnepf. 2014. Recovering root system traits using image analysis exemplified by two-dimensional neutron radiography images of lupine. PLANT Physiol. 164(1): 24–35. doi: 10.1104/pp.113.227892.

Li, D. 2009. Report on China rural informatization. China Inf. Times 1: 72–84.

Lobet, G., L. Pagès, and X. Draye. 2011. A novel image-analysis toolbox enabling quantitative analysis of root system architecture. Plant Physiol. 157(1): 29–39. doi: 10.1104/pp.111.179895.

Majdi, H. 1996. Root sampling methods - applications and limitations of the minirhizotron technique. Plant Soil 185(2): 255–258. doi: 10.1007/BF02257530.

Mancuso, S. 2011. Measuring roots: an updated approach. Springer Science & Business Media.

Marsh, B.H., and J. Grove. 1992. Surface and subsurface soil acidity: Soybean root response to sulfate-bearing spent lime. Soil Sci. Soc. Am. J. 56(6): 1837–1842.

Monk, S. 2016. Raspberry Pi cookbook: software and hardware problems and solutions. Second edition. O'Reilly Media, Sebastopol, CA.

Pedregosa, F., G. Varoquaux, A. Gramfort, V. Michel, B. Thirion, et al. 2011. Scikit-learn: Machine learning in Python. J. Mach. Learn. Res. 12: 2825–2830.

Persson, H. 1990. Nutrient cycling in terrestrial ecosystems: field methods, application, and interpretation (A.F. Harrison, P. Ineson, and O.W. Heal, editors). Elsevier Applied Science, London ; New York.

Pierret, A., S. Gonkhamdee, C. Jourdan, and J.-L. Maeght. 2013. IJ_Rhizo: an open-source software to measure scanned images of root samples. Plant Soil 373(1–2): 531–539. doi: 10.1007/s11104-013-1795-9.

Polomski, J., and N. Kuhn. 2002. Root research methods. Plant Roots Hidden Half 3: 295–321.

Pound, M.P., A.P. French, J.A. Atkinson, D.M. Wells, M.J. Bennett, et al. 2013. RootNav: Navigating images of complex root architectures. Plant Physiol. 162(4): 1802–1814. doi: 10.1104/pp.113.221531.

Precht, E., U. Franke, L. Polerecky, and M. Huettel. 2004. Oxygen dynamics in permeable sediments with wave-driven pore water exchange. Limnol. Oceanogr. 49(3): 693–705.

Rahman, G., H. Sohag, R. Chowdhury, K.A. Wahid, A. Dinh, et al. 2020. SoilCam: A fully automated minirhizotron using multispectral imaging for root activity monitoring. Sensors 20(3): 787. doi: 10.3390/s20030787.

Revsbech, N.P., O. Pedersen, W. Reichardt, and A. Briones. 1999. Microsensor analysis of oxygen and pH in the rice rhizosphere under field and laboratory conditions. Biol. Fertil. Soils 29(4): 379–385. doi: 10.1007/s003740050568.

Rewald, B., L. Seehra, O. Hadar, A. Sofer, P. Baykalov, et al. 2020. Enabling next level research on roots: Automatizing Minirhizotron Image Acquisition and Analysis (NextMR-IAA) for Research and Agricultural Management

Rickelt, L.F., L. Askaer, E. Walpersdorf, B. Elberling, R.N. Glud, et al. 2013. An Optode Sensor Array for Long-Term In Situ Oxygen Measurements in Soil and Sediment. J. Environ. Qual. 42(4): 1267. doi: 10.2134/jeq2012.0334.

Roberti, J.A., M.D. SanClements, H.W. Loescher, and E. Ayres. 2014. Traceable calibration, performance metrics, and uncertainty estimates of minirhizotron digital imagery for fine-root measurements (B. Bond-Lamberty, editor). PLoS ONE 9(11): e112362. doi: 10.1371/journal.pone.0112362.

Rusek, J. 2001. Microhabitats of Collembola (Insecta: Entognatha) in beech and spruce forests and their influence on biodiversity. Eur. J. Soil Biol. 37(4): 237–244.

Sanner, M.F. 1999. Python: a programming language for software integration and development. J. Mol. Graph. Model. 17(1): 57–61.

Schnepf, A., D. Leitner, M. Landl, G. Lobet, T.H. Mai, et al. 2018. CRootBox: a structural–functional modelling framework for root systems. Ann. Bot. 121(5): 1033–1053. doi: 10.1093/aob/mcx221.

Sruthy, S., and S.N. George. 2017. WiFi enabled home security surveillance system using Raspberry Pi and IoT module. 2017 IEEE International Conference on Signal Processing, Informatics, Communication and Energy Systems (SPICES). IEEE, Kollam. p. 1–6

Steinaker, D.F., and S.D. Wilson. 2008. Scale and density dependent relationships among roots, mycorrhizal fungi and collembola in grassland and forest. Oikos 117(5): 703–710. doi: 10.1111/j.0030-1299.2008.16452.x.

Sumner, M. 1995. Amelioration of subsoil acidity with minimum disturbance. In 'Subsoil management techniques'.(Eds NW Jayawardane, BA Stewart) pp. 147--185.

Svane, S.F., E.B. Dam, J.M. Carstensen, and K. Thorup-Kristensen. 2019. A multispectral camera system for automated minirhizotron image analysis. Plant Soil 441(1–2): 657–672. doi: 10.1007/s11104-019-04132-8.

Tang, C., Z. Rengel, E. Diatloff, and C. Gazey. 2003. Responses of wheat and barley to liming on a sandy soil with subsoil acidity. Field Crops Res. 80(3): 235–244.

Taylor, A.R., and A.J. Bloom. 1998. Ammonium, nitrate, and proton fluxes along the maize root. Plant Cell Environ. 21(12): 1255–1263. doi: 10.1046/j.1365-3040.1998.00357.x.

Taylor, H., D. Upchurch, and B. McMichael. 1990. Applications and limitations of rhizotrons and minirhizotrons for root studies. Plant Soil 129(1): 29–35.

Tovar, J.C., J.S. Hoyer, A. Lin, A. Tielking, S.T. Callen, et al. 2018. Raspberry Pi-powered imaging for plant phenotyping. Appl. Plant Sci. 6(3): e1031. doi: 10.1002/aps3.1031.

Upton, E., and G. Halfacree. 2012. Raspberry Pi user guide. John Wiley & Sons, Chichester, England.

Vamerali, T., M. Bandiera, and G. Mosca. 2012a. Minirhizotrons in Modern Root Studies. Measuring Roots. Springer, Berlin, Heidelberg. p. 341–361

Vamerali, T., M. Bandiera, and G. Mosca. 2012b. Minirhizotrons in Modern Root Studies. Measuring Roots. Springer, Berlin, Heidelberg. p. 341–361

Vicensi, M., C. Lopes, V. Koszalka, R.C. Umburanas, J.C.B. Vidigal, et al. 2020. Soil fertility, root and aboveground growth of black oat under gypsum and urea rates in no till. J. Soil Sci. Plant Nutr. 20(3): 1271–1286. doi: 10.1007/s42729-020-00211-3.

Wang, H., Y. Inukai, and A. Yamauchi. 2006. Root development and nutrient uptake. Crit. Rev. Plant Sci. 25(3): 279–301. doi: 10.1080/07352680600709917.

Wenzhöfer, F., and R.N. Glud. 2004. Small-scale spatial and temporal variability in coastal benthic O2 dynamics: Effects of fauna activity. Limnol. Oceanogr. 49(5): 1471–1481.

Wilson, S.D. 2014. Below-ground opportunities in vegetation science (R. Kalamees, editor). J. Veg. Sci. 25(5): 1117–1125. doi: 10.1111/jvs.12168.

Yan-e, D. 2011. Design of intelligent agriculture management information system based on IoT. 2011 Fourth International Conference on Intelligent Computation Technology and Automation. IEEE, Shenzhen, China. p. 1045–1049

Zeng, G., S.T. Birchfield, and C.E. Wells. 2008. Automatic discrimination of fine roots in minirhizotron images. New Phytol. 177(2): 549–557. doi: 10.1111/j.1469-8137.2007.02271.x.

Zhu, J., K.M. Brown, and J.P. Lynch. 2010. Root cortical aerenchyma improves the drought tolerance of maize (*Zea mays* L.). Plant Cell Environ. doi: 10.1111/j.1365-3040.2009.02099.x.

Chapter 2 - Benchmarking the RhizoPi automated minirhizotron camera system

Abstract

Understanding plant roots and root growth is critical for agricultural productivity as roots influence many plants, ecosystems, and biogeochemical processes. However, investigating root development in situ can be challenging. Minirhizotrons are generally used for root monitoring and allow non-destructive tracking of root development over time. Existing commercial minirhizotron cameras are costly and manually operated. We developed an inexpensive, automated minirhizotron camera system, the RhizoPi camera, built using off-the-shelf computer components. The purpose of this study was to evaluate the capability and utility of the RhizoPi camera system. The objectives were to 1) assess the capabilities and design of the RhizoPi minirhizotron camera system and benchmark it against a commercial minirhizotron camera; 2) create an image analysis script to analyze minirhizotron images and compare results to those of existing commercial software. Images collected using the RhizoPi camera system were examined for the percentage of the image that is roots (root percentage) using a script written in the Python programming language and the commercial minirhizotron image analysis program, RootSnap!®. The average root percentage measured by the Python script, 3.36%, was significantly larger than with RootSnap!, 2.97%, though the difference was slight in magnitude (0.39%). Images collected using the RhizoPi camera were compared to images collected on the same day using the commercially available CID Bioscience CI-600 minirhizotron camera. Images from the two camera systems were processed to ensure the exact image frame location was being compared, then processed using RootSnap! The two systems (RhizoPi/Python script) and (CI-600/RootSnap!) were not significantly different, thus validating our inexpensive system for

research analysis. Therefore, the RhizoPi camera system produces commercial-quality root imagery despite the low cost and use of off-the-shelf computer components.

Introduction

Roots play a critical role in carbon and nutrient cycling in soils (Eshel and Beeckman, 2013; Kirkham, 2014). Expanding our knowledge of rooting dynamics is crucial for progressing soil science, plant biology, agronomy, and related disciplines. One important instrument used to study rooting dynamics is minirhizotrons.

Minirhizotrons are transparent tubes inserted into auger holes in the soil that help image roots using cameras inserted into the tubes (Taylor et al., 1990b). Minirhizotrons and minirhizotron cameras are commonly used for in situ monitoring of roots and facilitate non-destructive tracking of root metrics over time (Bates, 1937). However, existing commercial cameras are expensive, usually require manual operation, and have significant labor requirements for image analysis (Persson, 1990; Zeng et al., 2008; Vamerali et al., 2012b).

The development of a low-cost, automated minirhizotron camera system can help overcome these challenges. The “RhizoPi” minirhizotron camera system was recently developed by the Root Ecology and Hydropedology Laboratory at Kansas State University. It is a fully automated minirhizotron camera that takes non-destructive, high resolution, digital pictures of the roots and the belowground environment. The camera, presented in the study below, is built using primarily off-the-shelf hardware and computer components, in addition to 3D-printed parts. This camera operates and takes pictures using software written in the open-source Python programming language. The total cost for parts is approximately $300 per camera for all parts, which is significantly cheaper than commercial minirhizotron cameras that exceed $20,000 per

camera. The low cost of this new camera system facilitates the permanent installation of minirhizotron cameras in the field, which in turn facilitates automated image collection on pre-determined time intervals.

The goals of this study were to 1) assess the capabilities and design of the RhizoPi minirhizotron camera system and benchmark that camera system against a commercial minirhizotron camera, and 2) test the algorithm developed to analyze minirhizotron images against an existing commercial minirhizotron image analysis software program.

Material and Methods

Greenhouse experiment

This experiment occurred during the spring of 2021 in a controlled greenhouse environment at Kansas State University in Manhattan, Kansas, USA. The imposed treatments were a randomized complete block designed with in-furrow arbuscular mycorrhizal fungi (AMF) and control. Since the images did not present any AMF infestation, we kept with the camera comparisons as the only treatments. It was designed to facilitate two comparisons. First, a comparison of the RhizoPi camera system to the CI-600 commercial camera system (CID Bioscience, Inc., Camas, WA, USA) using the same image analysis software, RootSnap! ® (CID Bioscience, Inc., Camas, WA, USA) for all image analyses. The second comparison was between camera systems (camera hardware and software) in which the RhizoPi camera with images analyzed using a script written in the Python programming language was compared to the CI-600 camera with images analyzed using the RootSnap! program. *Glycine max* (L.) Merr. (soybeans) was chosen as the study species for this experiment.

Soybean roots were imaged using both minirhizotron cameras. The CI-600 consists of a scanning head that spins inside the tube, capturing images 22 cm tall and 19.56 cm wide that represents nearly the full circumference of the minirhizotron tube. The camera is manually moved between each of the four positions inside of the tube using an indexing handle. The RhizoPi camera system operates differently, and consists of a camera that is horizontally stationary and captures an area representing two centimeters of circumference on the tube exterior (approximately 30% of the tube). However the RhizoPi camera is automated and moves downward incrementally, capturing images 1.25 cm in height at each stopping position along the length of the tube. Thus, roots were imaged using the CI-600 camera at depth intervals of 0 to 22 cm, 22 to 44 cm, 44 to 66 cm, and 66 to 88 cm; and imaged using the RhizoPi camera in 1.0 cm increments (ensuring overlap between each 1.25 cm tall image) to 88 cm in depth. These images were divided in two groups (0-50 cm and 50-100 cm) for data analysis.

Soybeans were grown in large polyvinyl chloride (PVC) columns that were 100 cm tall and 20 cm in diameter. A minirhizotron tube (6.35 cm diameter x 105 cm long) was inserted into each column, then the columns were packed with approximately 37 kg each of potting soil (Pro-Mix CC40 W/Mycorrhizae) reaching an approximate bulk density of 0.15 g cm^{-3}. To ensure that the exact image frame location to be compared, two stripes of dot marks were made along the exterior of the minirhizotron tubes using a rotary tool, resulting in a series of adjoining rectangles 2.5 cm wide (along the circumference of the tube) and 1 cm tall (Figure 2.1) from the top to the bottom of the tube. Soybeans were sown with three seeds per column then thinned to one seedling after germination. The soybean genotype used was KS4117NS (Kansas AES, Manhattan, KS, USA) maturity group four. The ten PVC columns were set up in two rows with 15 cm of distance between plants within rows, and 70 cm distance between rows.

Each column was irrigated with 200 mL tap water per day using a drip irrigation system. The greenhouse temperature was set to be 18.3°C at night and 26.7°C during the day. The photoperiod was set to promote flowering 50 days after planting, starting at 16 hours of daylight and dropping 1 hour every two weeks to reach 13 hours. Soybean plants were harvested at the second reproductive (R2) growth stage.

The camera-to-camera comparison was conducted by imaging the soybean roots on the same day using both cameras as described above. The images were then pre-processed by Python script to crop the images based on the dots at the corner of each rectangle and ensure the same image frame location was analyzed. Each image was analyzed using the "Estimate Root %" feature in the RootSnap! program which identifies the percentage of each image that is roots (root percentage). The camera comparison was made using the camera (CI-600 and RhizoPi) as pairwise t test grouped by root depth (0-50 and 50-cm) and also grouped by days after emergence (56 and 61 days after emergence).

The system-to-system comparison was conducted by the entire CI-600 system (hardware and software) and RhizoPi (hardware and software) as pairwise t test grouped by root depth (0-50 and 50-cm) and also grouped by days after emergence (56 and 61 days after emergence). The same comparison was made using the entire CI-600 system (hardware and software) and RhizoPi (hardware and software) as pairwise t test grouped by root depth (0-50 and 50-cm) and also grouped by days after emergence (56 and 61 days after emergence). In this case, each camera had the image analyzed using its own software.

Field experiment

The software-to-software comparison was performed using images from a field experiment using *Zea mays* L. (corn) with planned irrigation treatments that did not occur due to

the lack of necessity because of sufficient rainfall. In this case, the only treatments were the compared software (Python script and RootSnap!). The experiment was conducted during the 2020 corn growing season at the North Central Kansas Experiment Field in Scandia, Kansas, USA (39°49′54.56″N, 97°50′23.28″W). The field site is irrigated and has been managed as a long-term reduced tillage corn-soybean rotation for at least six years. The site was tilled in the early spring before planting, planted on April 21st with 76 cm row spacing and a seed population of 74,000 per hectare, and harvested on October 5th, 2020.

The soil is classified as Crete silt loam (Fine, smectitic, mesic Pachic Udertic Argiustolls). The weather is temperate. Average seasonal temperatures (maximum and minimum; °C), and cumulative precipitation (mm) were collected from a weather station from the Kansas Mesonet Network and are presented in Appendix Figure 2.1 and Appendix Table 2.1. The corn hybrid used was Pioneer P1828AM. Nitrogen application rates were balanced for the whole experiment and applied when the field was tilled for a total of 200 kg N ha^{-1} applied.

Minirhizotron tubes were installed in the field within seven days of plant emergence. Each treatment plot followed the east-west orientation of the rows, was 4.6 by 15.2 m in size encompassing six rows total. Two minirhizotron tubes were installed in the middle two rows between the harvested area at the center and the plot boundaries. A motor-powered, handheld auger and wooden jig were used to bore holes approximately 7.5 cm in diameter and 90 cm long at a 60° angle from the soil surface in the plant row (Figure 2.2). A one and a half meter acrylic minirhizotron tube with a waterproof plug at the base was embedded into each auger hole. PVC caps were used to seal the exposed tubes, regulate the light interference, and keep the imaging exterior clean and dry. Tubes were anchored in place with wooden stakes and plastic ties to prevent the tube raising with the water table in case of rain events.

The RhizoPi cameras were installed into the tubes and remained in the field. Root images were collected using the RhizoPi and CI-600 camera systems on the same day on a weekly basis throughout the growing season. The RhizoPi cameras were removed during CI-600 imaging and then replaced. The images capture an area two centimeters wide and 1.25 centimeters long with a resolution of 64 dots mm^{-1} (600 DPI resolution). The cameras were powered from batteries kept charged by solar panels installed in each plot. The cameras were controlled using either a tablet or laptop computer (Figure 2.3). Images were collected at ten depth positions along each tube. Those images were later analyzed for root percentage using both RootSnap! and the Python script (Appendix Code 2.1).

Images collected for this comparison were grouped into two depths, 0-50 and 50-100 cm depth and six image collection events: 55, 72, 80, 86, 92, and 115 days after emergence. The software comparison (Python script vs. RootSnap!) was made using the pairwise t test to compare images grouped by root depth and days after emergence. Ten images at ten different depths were taken per nine minirhizotron observation tubes during six imaging sessions from V4 to R1 (or DAE), resulting in 540 images total. To quantify root percentage by depth, the images were subjected to both RootSnap! and Python script (Appendix Code 2.1), processed to the percent area of root related to the image size. Each image's physical size was given in both pixels (1280 x 720) and centimeters (2 x 1.25), allowing for calculating pixels/cm scale.

Statistical analysis

The data from the greenhouse and field experiments were both tested for normality using the Shapiro Wilk test (Shapiro and Wilk, 1965), and tested for homogeneity of variance using the Levene test (Glass, 1966). The greenhouse data was normally distributed, but field experiment data was not. Thus, a normalization process was applied to the data using the square root of the

values of the quantitative variables. After being transformed, the data again went through the normality and homogeneity tests and passed.

The t-test for independent and paired measures was applied to perform the comparative analysis, the multiple comparison analysis - ANOVA with post hoc Tukey. Correlation and linear regression analyses also were applied to the data to characterize relationships between the quantitative variables (Figure 2.4). In addition to these, agreement analysis between the methods was applied using the Conbrach's alpha test to measure the internal consistency of the data.

Results

Minirhizotron camera comparisons

The RhizoPi camera had comparable results to those from the CI-600 camera in the greenhouse experiment involving soybean roots. Three sets of example images for both cameras from the same location and same day are presented in Figure 2.6. The mean root percentage determined using Rootsnap! was 10.67 % (±3.37%) for the RhizoPi camera, which was greater than the 9.92% (±3.84%) found using the CI-600 (Figure 2.5). That difference was significant ($p=0.02$), but was small in magnitude (0.89% ±3.44).

Exploring this difference by days after emergence we found a significant difference ($p=0.03$) between the RhizoPi (9.57% ±3.62%) and CI-600 (8.52% ±3.57%) cameras at 56 days after emergence, though there was no longer a significant difference by 61 days after emergence ($p=0.25$) (Figure 2.7). In comparing cameras by depth, there was no significant difference ($p=0.24$) between the two cameras at the 0-50 cm depth, but there was ($p=0.01$) at the 50-100 cm depth. In these deeper depths the RhizoPi root percentage (11.90% ±3.23%) was greater than the CI-600 (9.86% ±3.92%) (Figure 2.8). The results comparing both cameras using the RootSnap! software including measurements between dates and depths are presented on

Table 2.1.

Minirhizotron Camera System Comparisons

The two cameras were also compared as a minirhizotron camera system in which the images from each camera were analyzed using the respective image analysis software program (The RhizoPi camera and the Python script versus the CI-600 camera and RootSnap!). Three sets of example images for both software programs from the same image frames are presented in Figure 2.10, which is visible a similar pattern on identifying roots from both software. This was performed using the soybean root images in the greenhouse study. Across all images there was no significance difference ($p=0.56$) in root percentages observed between the two systems (Figure 2.9). The mean root percentages were 9.53% (±4.07) for the RhizoPi using the Python script and 9.28% (± 3.84) for the CI-600 using RootSnap!.

However, there were differences observed when comparing the systems for a given imaging session (Figure 2.11). At 56 days after emergence the RhizoPi/Python script system root percentage (11.32% ± 2.87%) was significantly greater ($p=<0.001$) than the CI-600/RootSnap! system (8.52% ±3.57%). This difference had reversed by 61 days after emergence where the CI-600/RootSnap! system (11.33% ± 3.62) had a significantly greater ($p=<0.001$) root percentage than the RhizoPi/Python script system (7.78% ± 4.39). Conversely, when the two systems were compared by depth (Figure 2.12), no significant differences were observed at either the 0-50 cm ($p=0.33$) depth or the 50-100 cm ($p=0.05$) depth. The results comparing both systems including measurements between dates and depths are presented on Figure 9 and Table 2.2.

Image analysis software comparisons

In the field study in which corn root images taken using the RhizoPi camera were analyzed by both the Python script and RootSnap!, a small (0.38%) but significant difference

(p=<0.001) between the two image analysis programs was detected (Table 2.3 and Figure 2.13). The average root percentage measured using the Python script was 3.35% (±0.69%), and the root percentage measured using Rootsnap! was 2.97% (±0.97%). Although that difference was significant, an agreement analysis was applied to identify whether results from the two programs were consistent. It determines how closely related a set of items are as a group to measure the scale reliability of the data. A Cronbach's alpha value of 0.6146 was found, indicating moderate internal consistency between the Python script and the RootSnap! software (Table 2.6). According to the Cronbach (1951) criterion, alpha values depict "almost perfect" internal consistency at values greater than 0.8, moderate consistency between 0.6 and 0.41, reasonable between 0.4 and 0.21, and small less than 0.21.

Observing the analysis from both software within different days after emergence, it was possible to find that there were significant differences on most of the dates which are reported on Table 2.3.

Grain yield

Average yields for corn in 2020 was 83.38 kg/ha per plot (15.24 m long x 4.57 m wide).

Discussion

The RhizoPi minirhizotron camera system performed comparably to the CI-600 minirhizotron camera. The images produced by the RhizoPi camera have excellent quality and at a higher default resolution than the CI-600. One advantage of the CI-600 camera is it images nearly the entire circumference of the minirhizotron tube, producing an image 21.59 cm in length by 19.56 cm of tube circumference. However, disadvantages of that camera are that it is significantly more expensive, has to be manually operated, and operates slowly in order to get the highest resolution possible (23.6 dots mm^{-1}). The RhizoPi camera is low cost and operates

automatically, producing high resolution (64 dot mm^{-1}) images. This disadvantage of the RhizoPi camera is it captures a smaller amount of the circumference of the minirhizotron tube, resulting in a strip of imaged area covering nearly the full length of the tube, but only 2 cm wide. However, this small area imaged can be overcome by adding additional cameras to the RhizoPi platform that are oriented towards different sections of the minirhizotron tube.

A comparison of the two cameras was performed using image analysis in greenhouse and field experiments. The camera-to-camera comparison, using the same software (RootSnap!) showed that there was a small in magnitude, yet significant difference in root percentage with the RhizoPi produced images that resulted in greater root percentages than for images produced by the CI-600. This can be attributed to the greater resolution in the RhizoPi (64 dots mm^{-1}) camera compared to the CI-600 (23.6 dots mm^{-1}) (Table 2.7) due to a more detailed image that helps the software to better track the root percentages. In addition, the LED light and the Raspberry PI NOIR (no infrared filter) camera used in the RhizoPi presented a brighter image (Figure 2.6), which may contribute to greater contrast in the images, leading to a greater detection of roots. Roberti et al. (2014) observed a limitation from the CI-600 when resolving smaller objects, which could stem from limited contrast in CI-600 images.

We found no statistical difference overall between the RhizoPi/Python script system and the CI-600/RootSnap! systems. Thus, the question remains whether there is a difference between the hardware or the software or even both. This is a critical point, because lack of agreement between minirhizotron camera systems may lead to minirhizotron studies not being comparable. Therefore, we decided to compare the same images from the RhizoPi camera for different software (Python script and RootSnap!) and we found no difference between software programs on root percentage area. This lack of difference may be attributed to the threshold settings for

both software programs, which are set by the user and help adapt the software programs to the respective image quality.

Exploring differences found between the two software programs for the same images, we found that the Python script produced greater root percentages than RootSnap!, though that difference was small in magnitude. This result can be attributed to the fact that the Python script is an automated system, while the RootSnap! program requires a person to operate the software to determine root percentage. Because one of the minirhizotron tube drawbacks is that the water can condense (Böhm, 1979) on the tube surface, the automated Python script may falsely count condensation as roots, and thus overestimate root percentages. In this case, the RootSnap! avoids some overestimated root percentages considering its manual operation. Further improvements to the Python script will be necessary to reduce non-root features from being counted as roots.

The difference attributed to the software may be related to its parameterization. In this case, the parameterization criteria for the RootSnap! agrees with the visualization of the Pearson correlation coefficient (0.46) (Table 2.6). The parameterization criteria for the RhizoPi software used the CV2 package from Python with morphological transformations. Thus, these transformations are simple operations based on the image shape for making boundaries of the foreground object, such as soil and roots (Figure 2.10). The fact that we do not have a reference value for the actual percentage of the root limits the assessment of the software's accuracy.

Although there is a difference between software and hardware of the systems, and the results of the same images using a different software, there is a correlation between results from both software (Figure 2.4). The fact of an existing proportionality between the values may indicate a relative precision and that eventually, both software will need calibration.

The observed differences between days after emergence and depth showed inconsistency, potentially due to analysis limitation between old and new roots. Some researchers have been trying to quantify the age and/or health of fine roots by color through image analysis, such as Dannoura (2008). However, the color nomenclature used by researchers to define root health is unstandardized and ambiguous (Roberti et al., 2014). Therefore, a calibration for the specific crop should be made before collecting data. In addition, growing roots in containers can obtain a different behavior when compared with field experiments.

With this innovation and permanently installed cameras, automation is now possible under in situ growing conditions or extensive mesocasm container studies. Even though minirhizotrons have expanded in utilization, there is still much to be discovered. Many previous studies have been small-scale or involved a limited number of species and at unique sites (Gregory, 2006; Wilson, 2014), which makes it harder to other species and locations (Kobiela et al., 2016). Therefore, more studies are necessary to examine multiple species and their interactions on the field to fill in some of the knowledge gaps of the world's diverse plant environments (Wilson, 2014).

Conclusion

The RhizoPi camera system was designed to use off-the-shelf components and 3D printed parts, costing about approximately $300 per camera. The design will be released as an open-source design, thus ensuring an affordable and accessible minirhizotron camera platform. This affordability of the RhizoPi camera combined with the automated operation may lead to increased use of minirhizotron cameras and root imaging that will facilitate computer visioning of roots. The key result from this study is that the RhizoPi camera design, in its current form,

produces imageries that are comparable to those produced by a commercial minirhizotron camera. Further, these imageries are produced using a camera designed for affordability and automated operation.

References

Bates, G. 1937. A device for the observation of root growth in the soil. Nature 139(3527): 966.

Böhm, W. 1979. Methods of studying root systems. Springer Science & Business Media.

Cronbach, L.J. 1951. Coefficient alpha and the internal structure of tests. Psychometrika 16(3): 297–334. doi: 10.1007/BF02310555.

Dannoura, M., Y. Kominami, H. Oguma, and Y. Kanazawa. 2008. The development of an optical scanner method for observation of plant root dynamics. Plant Root 2: 14–18. doi: 10.3117/plantroot.2.14.

Eshel, A., and T. Beeckman. 2013. Plant roots: the hidden half. CRC press.

Glass, G.V. 1966. Testing Homogeneity of Variances. Am. Educ. Res. J. 3(3): 187–190. doi: 10.3102/00028312003003187.

Gregory, P.J. 2006. Plant roots: growth, activity, and interaction with soils. Blackwell Pub, Oxford ; Ames, Iowa.

Kirkham, M.B. 2014. Principles of soil and plant water relations. Academic Press.

Kobiela, B., M. Biondini, and K. Sedivec. 2016. Comparing root and shoot responses to nutrient additions and mowing in a restored semi-arid grassland. Plant Ecol. 217(3): 303–314. doi: 10.1007/s11258-016-0571-3.

Persson, H. 1990. Nutrient cycling in terrestrial ecosystems: field methods, application, and interpretation (A.F. Harrison, P. Ineson, and O.W. Heal, editors). Elsevier Applied Science, London ; New York.

Roberti, J.A., M.D. SanClements, H.W. Loescher, and E. Ayres. 2014. Traceable calibration, performance metrics, and uncertainty estimates of minirhizotron digital imagery for fine-root measurements (B. Bond-Lamberty, editor). PLoS ONE 9(11): e112362. doi: 10.1371/journal.pone.0112362.

Shapiro, S.S., and M.B. Wilk. 1965. An analysis of variance test for normality (complete samples). Biometrika 52(3–4): 591–611. doi: 10.1093/biomet/52.3-4.591.

Taylor, H.M., D.R. Upchurch, and B.L. McMichael. 1990. Applications and limitations of rhizotrons and minirhizotrons for root studies. Plant Soil 129(1): 29–35. doi: 10.1007/BF00011688.

Vamerali, T., M. Bandiera, and G. Mosca. 2012. Minirhizotrons in Modern Root Studies. Measuring Roots. Springer, Berlin, Heidelberg. p. 341–361

Wilson, S.D. 2014. Below-ground opportunities in vegetation science (R. Kalamees, editor). J. Veg. Sci. 25(5): 1117–1125. doi: 10.1111/jvs.12168.

Zeng, G., S.T. Birchfield, and C.E. Wells. 2008. Automatic discrimination of fine roots in minirhizotron images. New Phytol. 177(2): 549–557. doi: 10.1111/j.1469-8137.2007.02271.x.

Figures and Tables

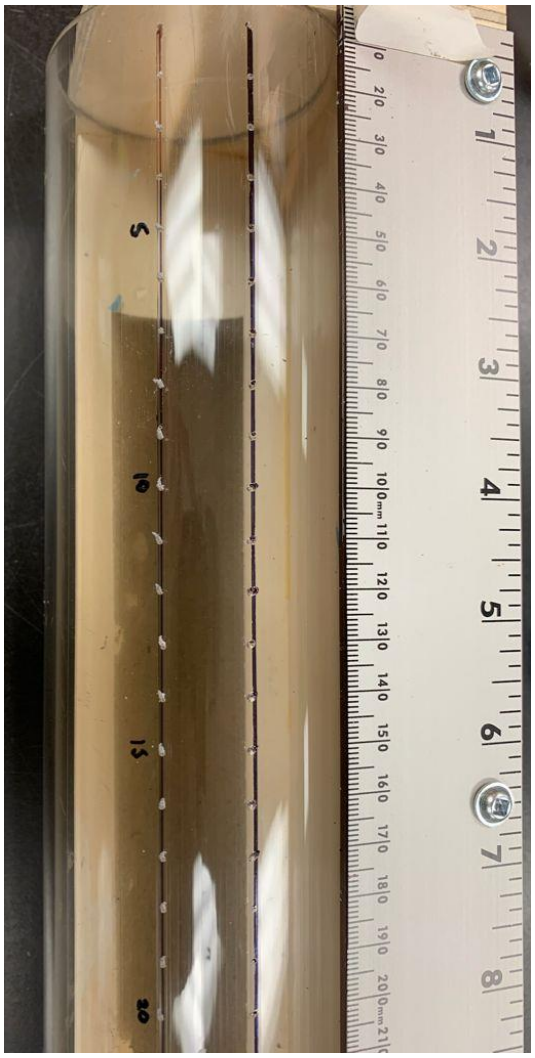

Figure 2.1. Minirhizotron tube with stripe dots to ensure the exact image frame location was being compared.

Figure 2.2. Installed minirhizotron with a 60° angle.

Figure 2.3. Field operation of the RhizoPi camera system.

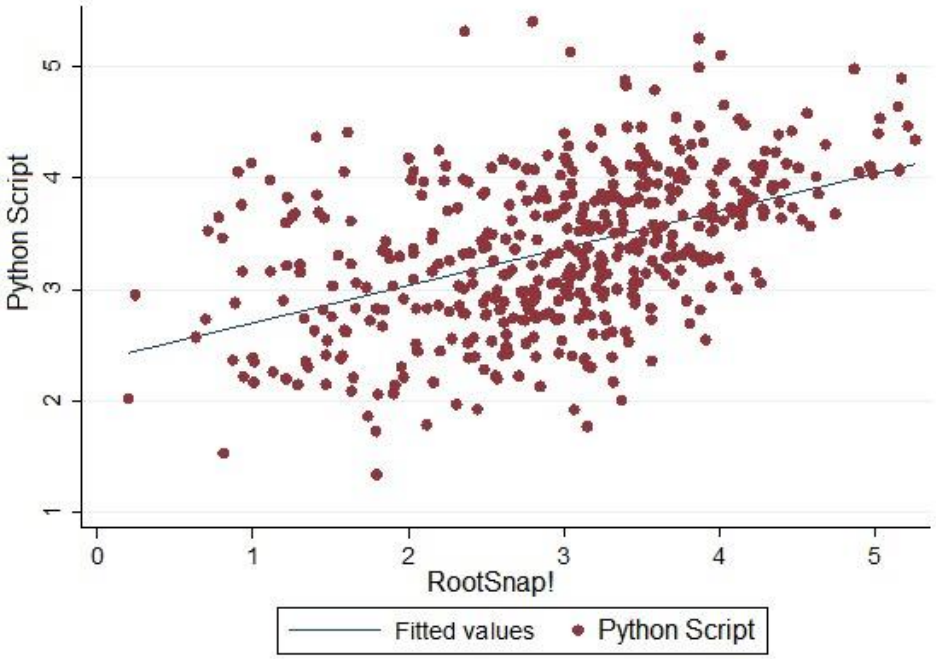

Figure 2.4. Estimated value for RhizoPi and RootSnap! regression.

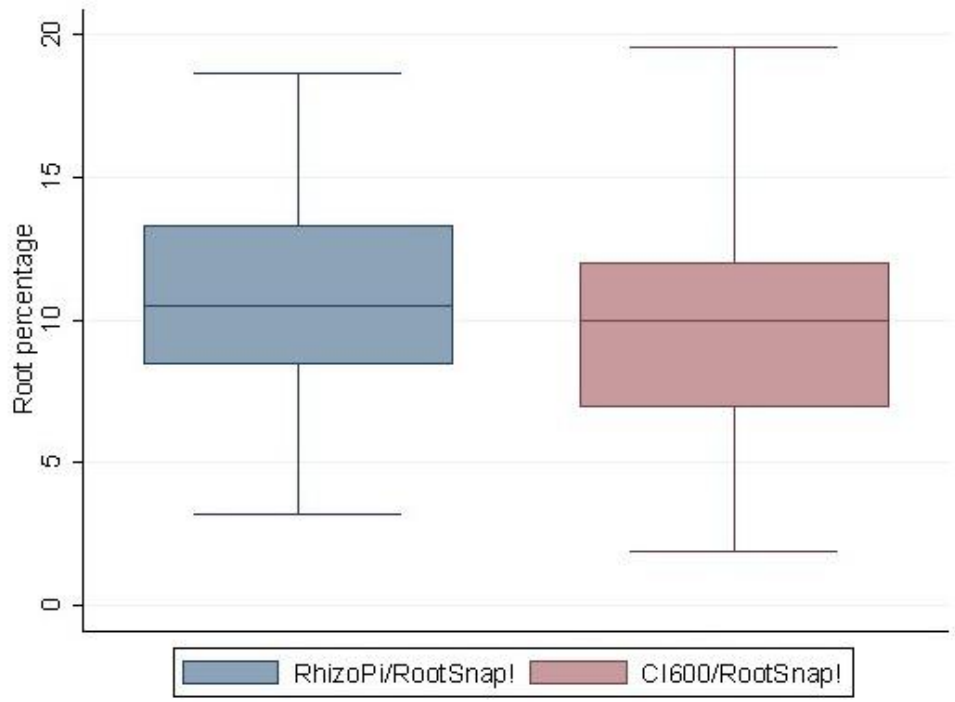

Figure 2.5. Comparing camera to camera (CI-600 x RhizoPi) using RootSnap! software.

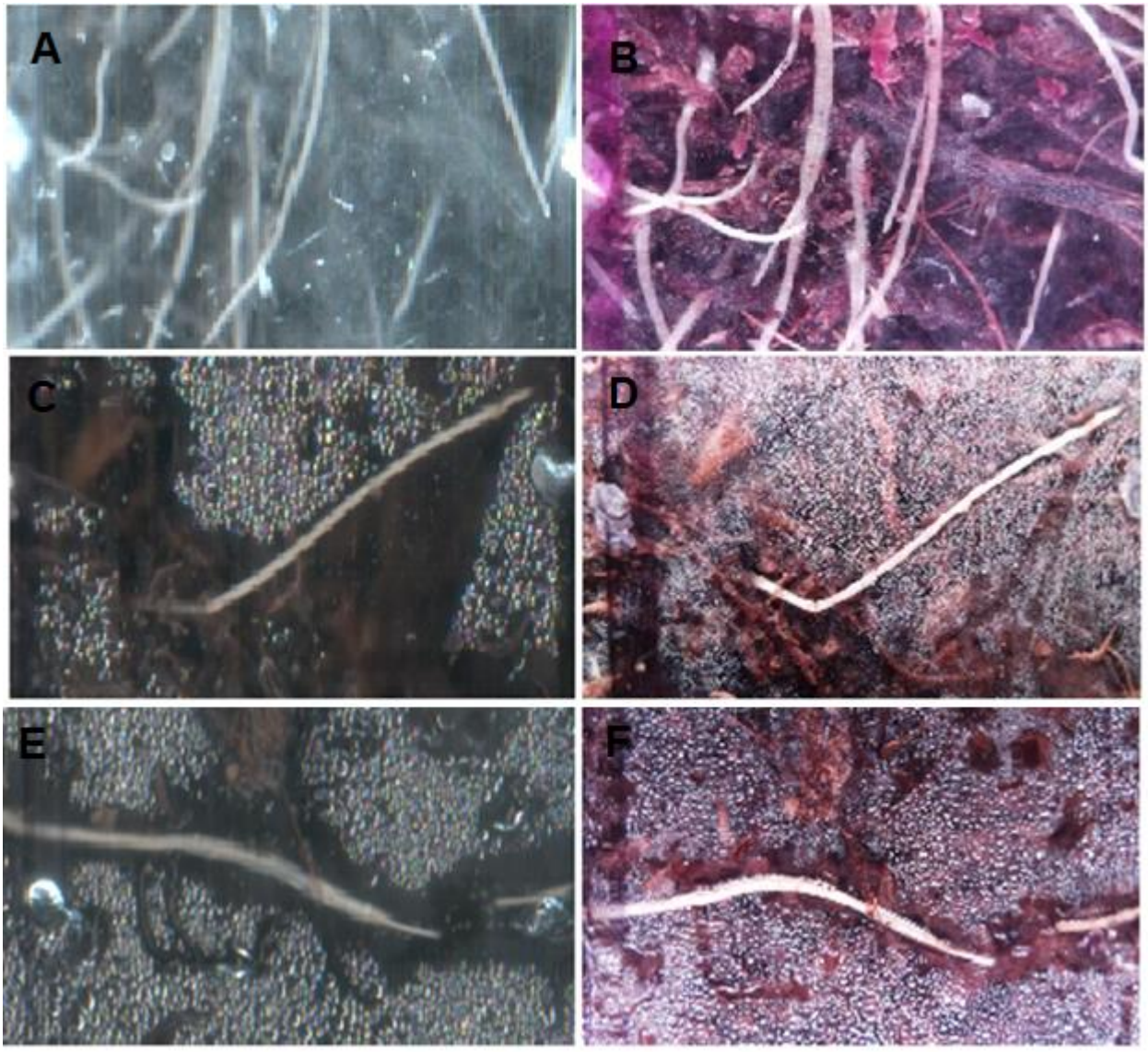

Figure 2.6. Camera comparisons. CI-600 (left) and the RhizoPi (right).

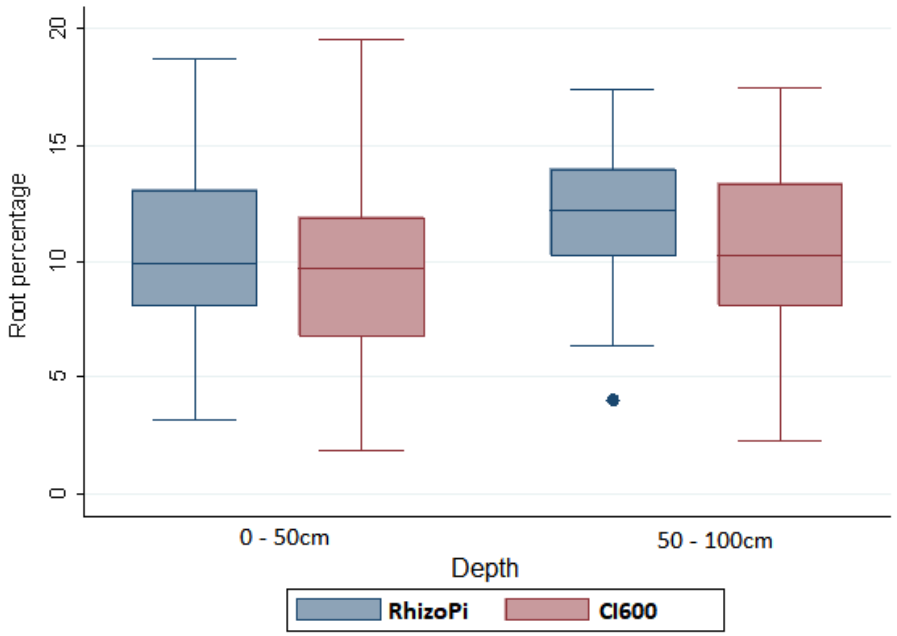

Figure 2.7. Comparing camera to camera (CI-600 x RhizoPi) using RootSnap! software for different days after emergence (56 and 61).

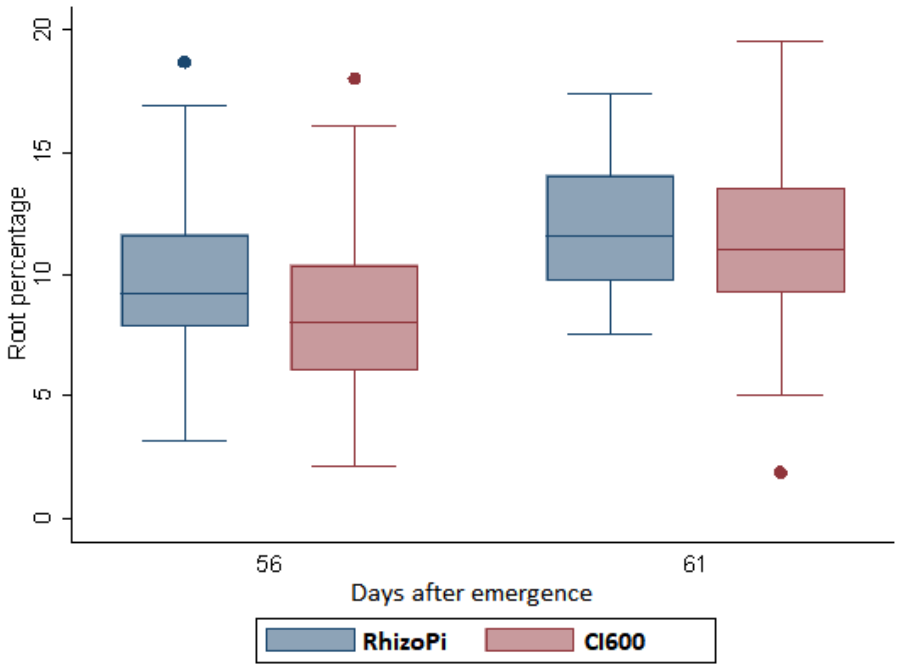

Figure 2.8. Comparing camera to camera (CI-600 x RhizoPi) using RootSnap! software for different depths (0-50 cm and 50-100 cm).

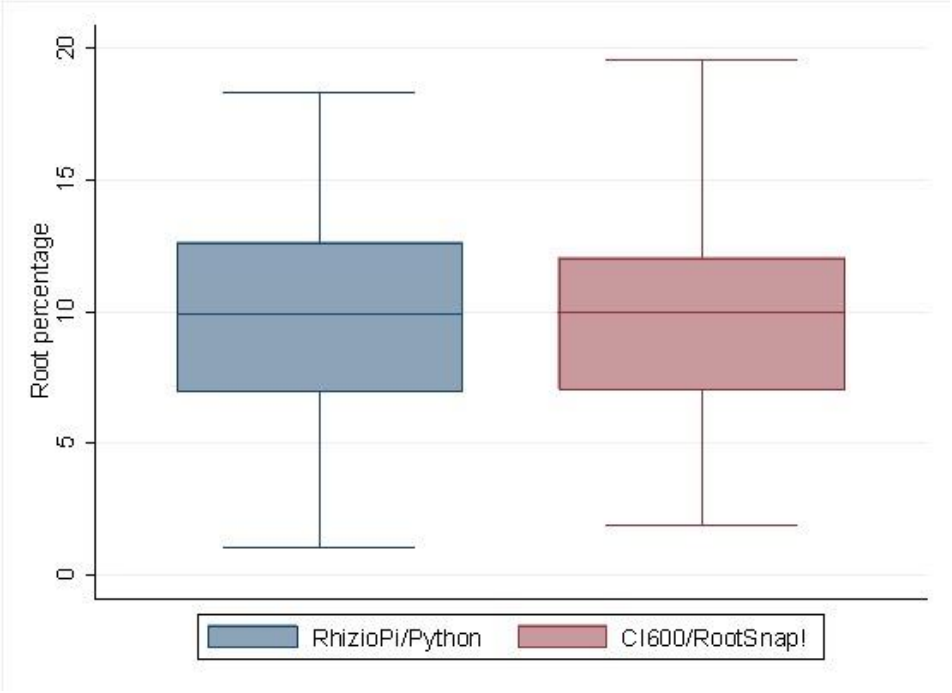

Figure 2.9. Comparing system to system (RhizoPi/Python script x CI-600/RootSnap!).

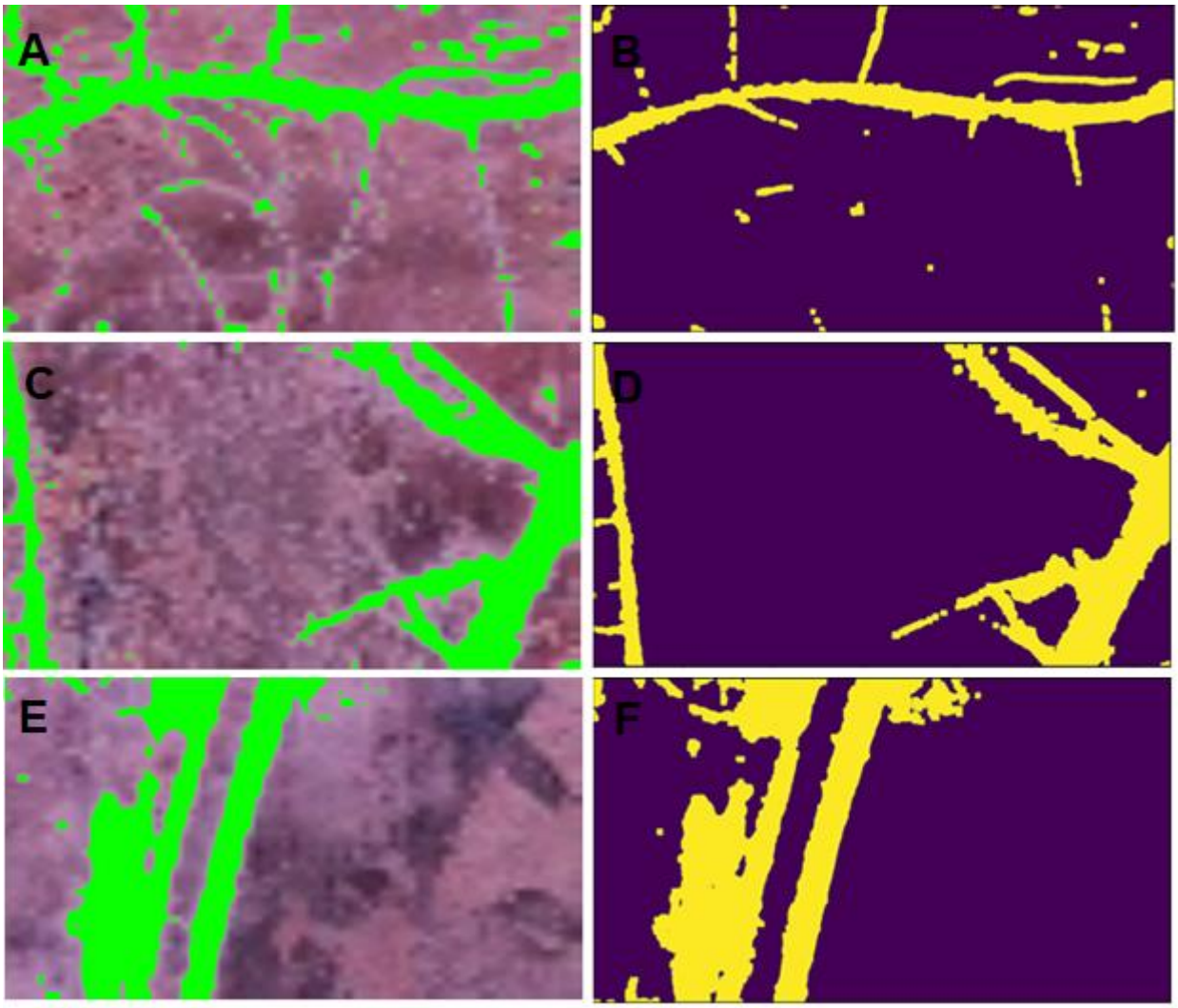

Figure 2.10. Software comparisons with RootSnap! (left) and Python script (right) images for the corn roots. The values of root percentage estimations were A- 14.31% and B-17.48%; C-17.8% and D-19.02%; E- 17.8% and F-19.02%.

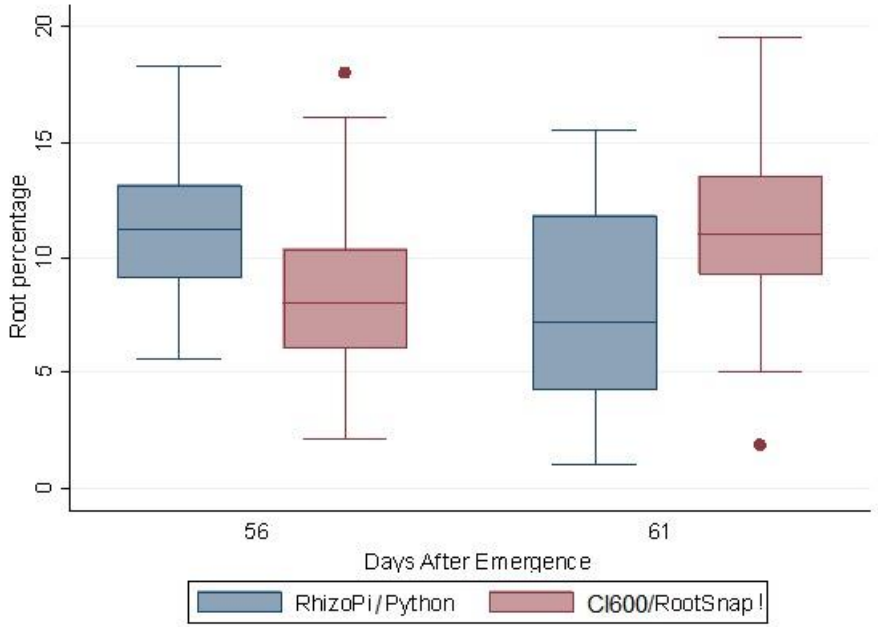

Figure 2.11. Comparing system to system (RhizoPi/Python script x CI-600/RootSnap!) for different days after emergence (56 and 61).

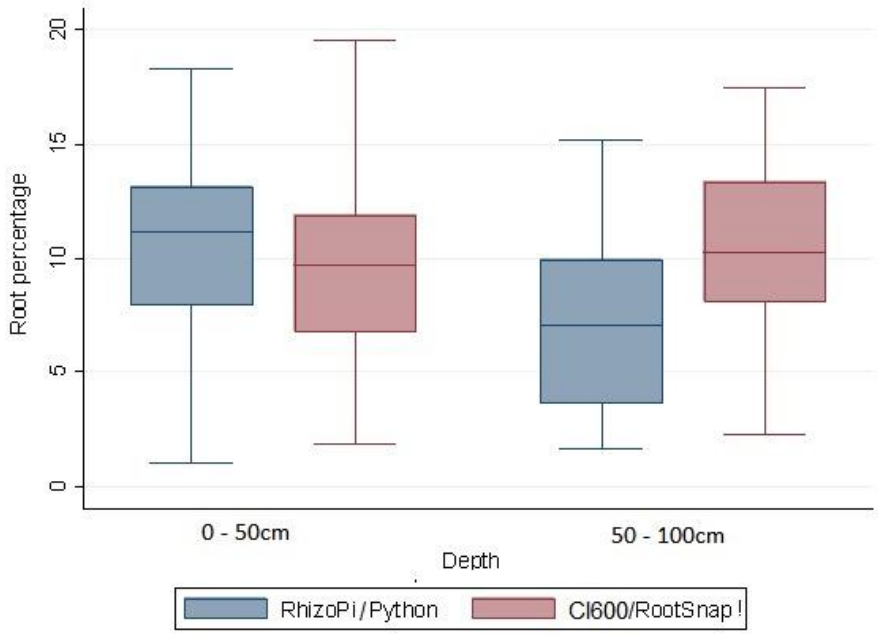

Figure 2.12. Comparing system to system (RhizoPi/Python script x CI-600/RootSnap!) for different depths (0-50 cm and 50-100 cm).

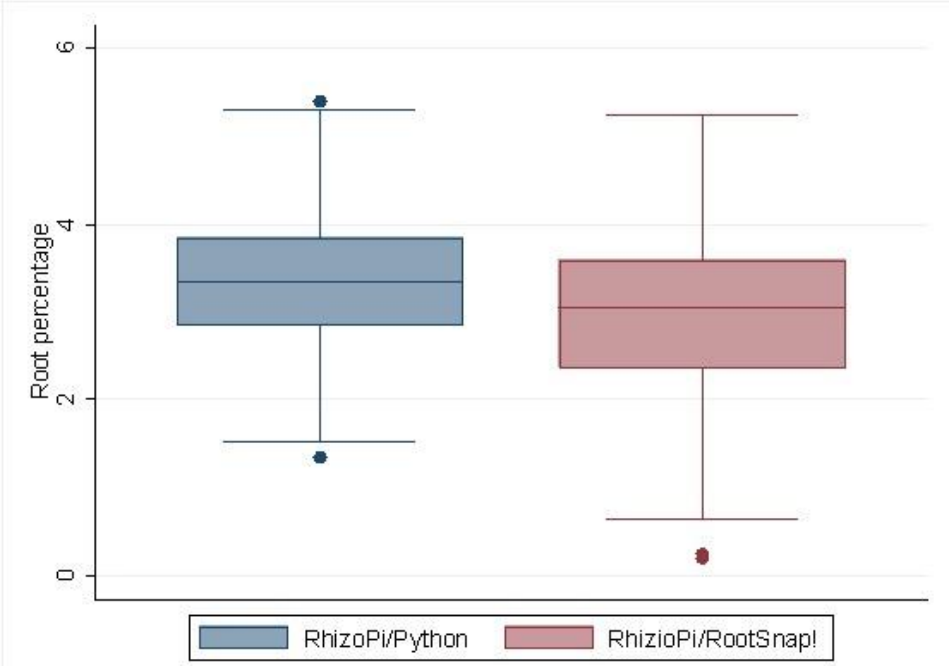

Figure 2.13. Comparing software to software (Python script x RootSnap!) for RhizoPi images.

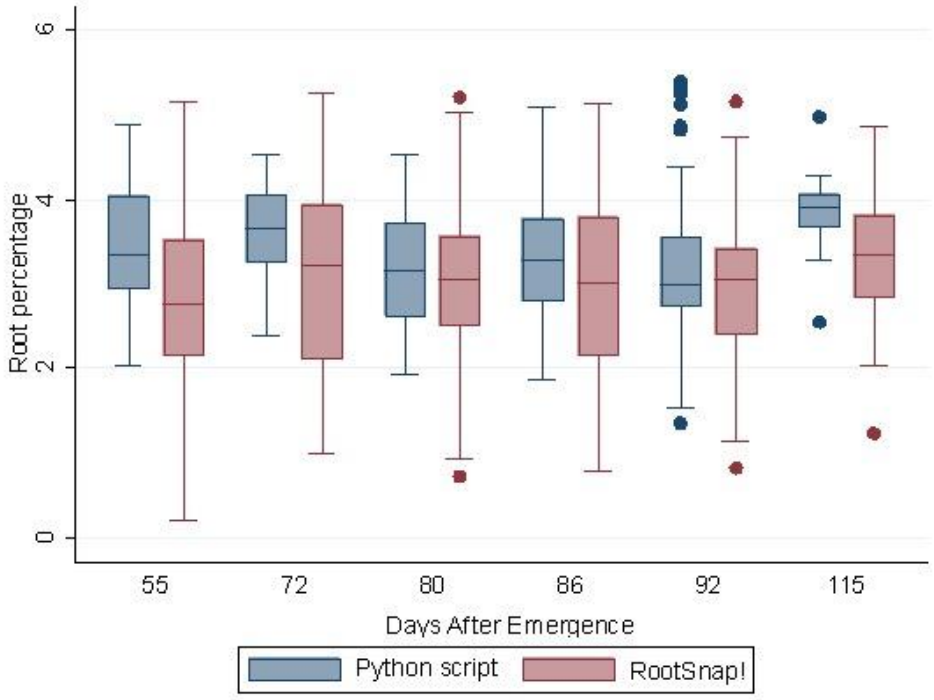

Figure 2.14. Distribution of camera software by days after emergence (DAE).

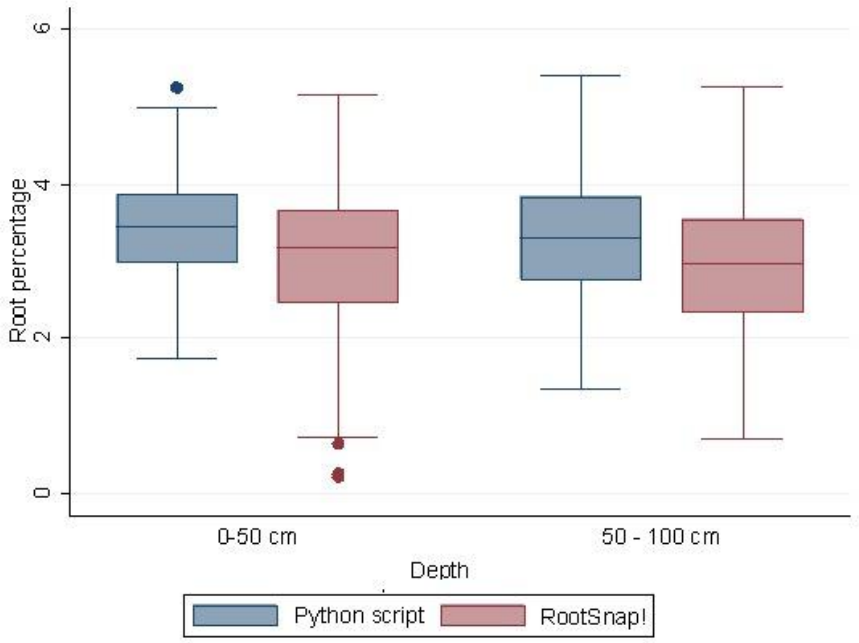

Figure 2.15. Comparison of two software (Python script x RootSnap!) for the RhizoPi images within depths.

Table 2.1. Camera comparison (CI-600 vs. RhizoPi) using RootSnap! software analysis of soybean root images from all dates and depths.

Camera			Days after emergence (DAE)				Depth (cm)			
			56		61		0-50		50-100	
	Mean (%)	SD	Mean (%)	SD	Mean (%)	SD	Mean (%)	SD	Mean (%)	SD
RhizoPi	10.67	3.37	9.57	3.62	11.76	2.58	10.14	3.31	11.9	3.23
CI-600	9.92	3.84	8.52	3.57	11.05	3.69	9.62	3.81	9.86	3.92
p-value	0.02		0.03		0.25		0.24		0.01	

Table 2.2. System comparison (RhizoPi/Python script vs. CI-600/RootSnap!) of soybean root images from all dates and depths.

System			Days after emergence (DAE)				Depth (cm)			
			56		61		0-50		50-100	
	Mean (%)	SD	Mean (%)	SD	Mean (%)	SD	Mean (%)	SD	Mean (%)	SD
RhizoPi/Python	9.53	4.07	11.32	2.87	7.78	4.39	10.48	3.78	6.93	3.79
CI600/RootSnap!	9.28	3.84	8.52	3.57	11.33	3.62	9.8	3.78	10.3	4.09
p-value	0.56		<0.001		<0.001		0.33		0.05	

Table 2.3. Paired comparison of image measurements.

Measurement	Mean **(%)**	Standard Deviation	
Python script	3.35	0.69	
RootSnap!	2.97	0.97	
Comparison	Mean Difference	Standard Deviation of the difference	p-value
CI600 x RhizoPi	-0.38	0.89	<0.001

*p-value for the paired comparison t-test; p-value <0.05 indicates statistical significance.

Table 2.4. Comparison of two softwares (Python script x RootSnap!) for the RhizoPi images within days after emergence.

	Software				
	Python script		RootSnap!		
Days After emergence	Mean (%)	SD	Mean (%)	SD	p-value
55	3.43	0.67	2.74	1.07	<0.001
72	3.62	0.55	3.08	1.04	<0.001
80	3.19	0.68	3.04	0.86	0.1170
86	3.30	0.67	2.94	1.09	<0.001
92	3.12	0.77	2.90	0.86	0.0106
115	3.85	0.37	3.33	0.75	<0.001

Table 2.5. Comparison of two softwares (Python script x RootSnap!) for the RhizoPi images within depths.

	Depth (cm)			
	0-50		50-100	
	Mean (%)	SD	Mean (%)	SD
Python script	3.41	0.65	3.29	0.73
RootSnap!	3.02	0.97	2.91	0.97
p-value	<0.001		<0.001	

Table 2.6. Description of agreement analysis between camera software.

(%)	Degrees of Agreement			Linear model			
Measurement	Python script	RootSnap!	Cronbrach's alpha	r	R^2	Equation	p-value (test F)
Model			0.61	0.4693 (<0.001)	21.86%	Y = 2.36 + 0.33X	<0.001
Minimum	1.79	0.04					
Mean	2.97	3.36					
Median	3.05	3.36					
Standard Deviation	0.78	0.69					
Maximum	29.16	27.61					

Cronbach's alpha regarding the agreement between the measures. In this case, 0.61 is a substantial amount.

Table 2.7. Camera's Feature and Specifications for CI-600 and RhizoPi hardwares.

Specifications	CI-600	RhizoPi
Image Size	21.59 cm × 19.56 cm (8.5 in × 7.7 in)	2.0 cm × 1.25 cm
Scan Speed	30-150 seconds depending on scanning resolution (3.9 dot/mm-23.6dot/mm)	5 seconds per image
Image Resolution	3.9, 11.8, and 23.6 dot/mm	720*1280 and 64 dot/mm
Computer	Handheld tablet	Laptop with self-made app
Software	CI-600 In-Situ Root Imager and RootSnap!	RhizoPi app and python programming language
Interface	USB Cable	Wi-Fi
Scan Head Dimensions	34.3 cm long × 6.35 cm diameter	40 cm long x 6.35 diameter
Scanner Unit Weight	0.75 kg	3 kg
System Requirements	Microsoft Windows XP, Vista, 7, 8, 10 1GB Memory/RAM 1GHZ+ Processor	2 Raspberry PI zero with +32GB SD card
Operation	Manually operated	Fully automated and manually operated modes
Cost	$18,000 total	$ 300 for parts $ 300 for labor

Appendix

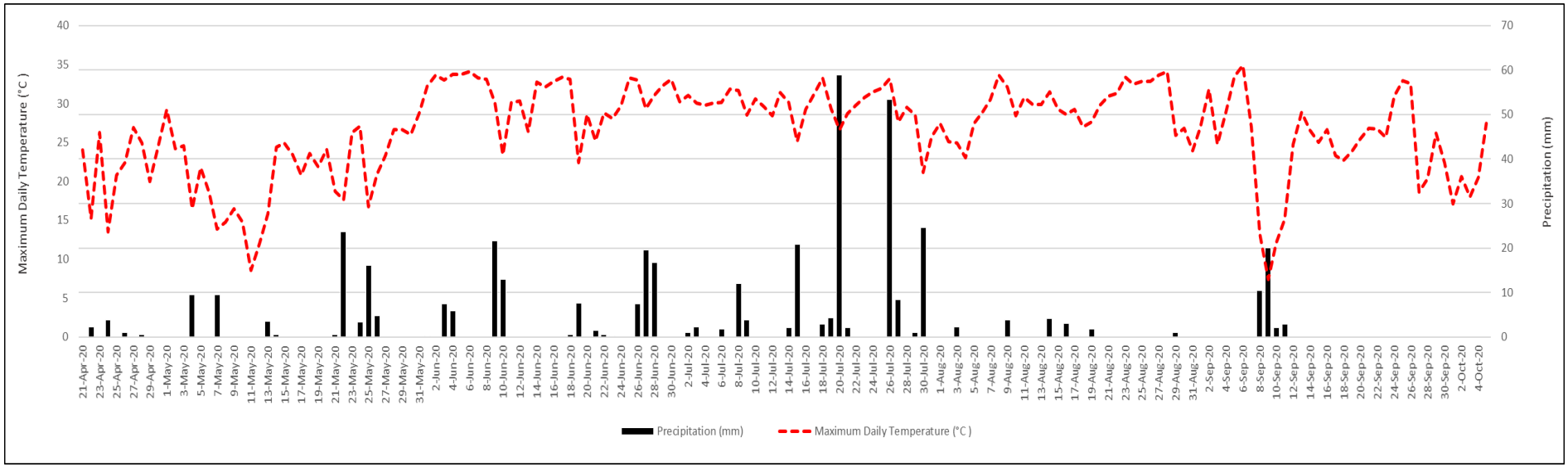

Appendix Figure 2.1. Daily precipitation and maximum temperature for the 2020 growing seasons at Scandia, KS.

Appendix Table 2.1. Scandia, KS weather data. Monthly average maximum temperature and total precipitation for 2020 (Kansas State University Mesonet, 2021).

Month	Average Maximum Temperature (˚C)	Average Minimum Temperature (˚C)	Average Precipitation (mm)
April	21.86	4.32	0.788
May	21.06	9.3	2.30
June	30.86	17.57	3,403
July	29.55	18.61	6,426
August	29.44	16.25	0.524
September	24.85	9.59	1,176
October	20.72	1.54	0

Appendix Table 2.2. Comparing camera to DAE (CI-600 x DAE) and (RhizoPi x DAE).

	Days after emergence (DAE)				
	56		61		
	Mean (%)	SD	Mean (%)	SD	p-value
CI-600	8.52	0.53	11.33	0.54	0.0004
RhizoPi	9.68	0.54	11.84	0.42	0.0033
Difference	-1.05	0.49	-0.70	0.60	0.65

*T test for comparison of independent groups

Both cameras showed increases in root percentages between the two imaging sessions (Appendix Table 2.2). A significant increase (p=0.0033) was observed from 9.68% (± 0.54) at 56 days after emergence to 11.84% (± 0.42) at 61 days after emergence using the RhizoPi camera. Similarly, a significant increase (p=0.0004) from 8.52% (± 0.53) to 11.33% (± 0.54) was observed using the CI-600 camera during the same imaging sessions, respectively.

Appendix Table 2.3. Comparing camera to depth (CI-600 x Depth) and (RhizoPi x Depth).

	Depth				
	0-50 cm		50-100 cm		
	Mean (%)	SD	Mean (%)	SD	p-value
CI-600	9.79	0.46	10.30	0.85	0.56
RhizoPi	10.28	0.42	11.90	0.72	0.06
Difference	-0.51	0.43	2.04	0.73	0.08

*T test for comparison of independent groups

As shown in Appendix Table 2.3, there was no significant difference between the 0-50 cm depth and the 50-100 cm depth for either the RhizoPi (p=0.06) or CI-600 (p=0.56) cameras.

Appendix Table 2.4. Comparing system to DAE (RhizoPi/Python x DAE) and (CI-600/RootSnap! x DAE).

	Days after emergence (DAE)				
	56		61		
	Mean (%)	SD	Mean (%)	SD	p-value
System					
RhizoPi/Python	11.27	0.42	7.75	0.64	<0.001
CI-600/RootSnap!	8.52	0.53	11.33	3.62	<0.001
Difference	2.8	0.56	-3.55	0.93	<0.001

The results of comparisons between imaging session within a given camera system are reported in Appendix Table 2.4. For RhizoPi/Python script system, the average root percentage significantly decreased (p=<0.001) from 11.27% (±0.42) at 56 days after emergence to 7.75% (±0.64) at 61 days after emergence. The CI-600/RootSnap! system significantly increased (p=<0.001) from 8.52% (±0.53) at 56 days after emergence to 11.33% (±3.62) at 61 days after emergence (Appendix Table 2.4).

Appendix Table 2.5. Comparing system to depth (RhizoPi/Python x Depth) and (CI-600/RootSnap! x Depth).

	Depth				
	0-50 cm		50-100 cm		
	Mean (%)	SD	Mean (%)	SD	p-value
System					
RhizoPi/Python script	10.46	0.46	6.93	0.77	0.0002
CI-600/RootSnap!	9.79	0.46	10.3	0.85	0.5913
Difference	0.68	0.70	-3.36	1.27	0.0049

*p-value <0.05 indicates statistical significance.

The results of comparisons of root percentages between the 0-50 cm depth and 50-100 cm depth for a given system is shown in Appendix Table 2.5. A significant difference (p=0.0002) between the 0-50 cm depth (10.46% ± 0.46) and 50-100 cm depth (6.93% ± 0.77%) was observed for the RhizoPi/Python script. However, no significant difference (p=0.5913) was observed between depths for the CI-600/RootSnap! system.

Appendix Table 2.6. Comparison between depth levels and software images.

	Depth				
	0-50 cm		50-100 cm		
	Mean (%)	Standard Deviation	Mean (%)	Standard Deviation	p-value
Python script	3.41	0.65	3.29	0.73	0.06
RootSnap!	3.02	0.97	2.91	0.97	0.21

*p-value for the t-test for comparison of independent groups; p-value <0.05 indicates statistical significance.

The comparison between depths for a given image analysis software program is shown in Appendix Table 2.6. No significant differences were observed between the 0-50 cm and 50-100 cm depths for either RootSnap! (p=0.21) or the Python script (p=0.06).

Appendix Code 2.1. Python code for percentage analysis

```
# import libraries
import cv2
import numpy as np
import matplotlib.pyplot as plt
from PIL import Image
import os, sys
import pandas as pd
import glob

# folder with images
path_to_folder = r'C:\\Users\\josecpp\\Desktop\\python_work\\All_files'

# list all images in the folder
imgs = glob.glob(path_to_folder + '/*.jpg')

# print listed imgs
print(imgs)

# define objects for dilation
kernel = np.ones((8,8), np.uint8)
kernel2 = np.ones((12,12), np.uint8)

# create an empty list to store the dilation of each img
_imgs = []
_csv = []

# loop through all imgs
for i in imgs: # i = imgs[0]

    print('Processing img: {0}'.format(i))

    # read img
    img = cv2.imread(i)

    ret,thresh1 = cv2.threshold(img,170,255,cv2.THRESH_BINARY)
    opening = cv2.morphologyEx(thresh1, cv2.MORPH_OPEN, kernel)
    erosion = cv2.erode(opening, kernel2, iterations = 1)
    dilation = cv2.dilate(erosion, kernel2, iterations = 1)

    # bands
    red = dilation[:,:,0]
    green = dilation[:,:,1]
    blue = dilation[:,:,2]

    # overall calculate root percentage
    overall_root_percentage = len(dilation[dilation>0])/dilation.size * 100

    red_rp = len(red[red>0])/red.size * 100
    green_rp = len(green[green>0])/green.size * 100
    blue_rp = len(blue[blue>0])/blue.size * 100


    # add img dilation to empty list
    _imgs.append(dilation)
```

```
    # add root_percentage to dictionary to create a panda data.frame

_csv.append({'img_id':i,'overall_root_percentage':overall_root_percentage,
                 'red_rp':red_rp,
                 'green_rp':green_rp,
                 'blue_rp':blue_rp})

    # save fig
    fig_name =
os.path.join('results',os.path.basename(i).replace('jpg','png'))

    fig = plt.figure(figsize=(10, 10))
    grid = ImageGrid(fig, 111,  # similar to subplot(111)
                     nrows_ncols=(2, 2),  # creates 2x2 grid of axes
                     axes_pad=0.5,  # pad between axes in inch.
                     )

    for ax, im, t in zip(grid, [red, green, blue, _imgs[-1]],title):
        # Iterating over the grid returns the Axes.
        ax.imshow(im)
        ax.set_title(t)

    fig.savefig(fig_name,dpi=300)

# csv with with root percentage
root_percentage_df = pd.DataFrame(_csv)
root_percentage_df.to_csv('results/dataframe.csv')
```

Chapter 3 - Minirhizotron based planar optodes

Abstract

Analyses of both rooting dynamics and soil solution chemistry are important for understanding belowground processes. Unfortunately, methods for monitoring root development and soil solution chemistry have been separated by location, time, or both, due to issues associated with sampling. Planar optical sensors (optodes) are an emerging technology that overcomes the hindrances of established sensors and technologies, and can be used to quantify environmental parameters. Planar optodes are non-invasive sensors that rely on fluorescent dyes that fluoresce at different intensities based on the concentrations of analytes dissolved in the soil solution. Planar optodes are a proven technology for quantifying concentrations of soil solutes, but the need for imaging the dyes through transparent surfaces has primarily restricted their use to laboratory settings. To date, planar optodes have not been coupled with minirhizotrons, which are transparent tubes inserted into auger holes in the soil. Minirhizotrons are traditionally used with cameras that are inserted into the tube to repetitively image roots in contact with the outside of the tube. We developed an inexpensive, automated minirhizotron camera system, the RhizoPi camera using off-the-shelf computer components. In this Chapter we present a method for using the RhizoPi camera system as a platform for imaging planar oxygen optodes on the exterior of minirhizotron tubes. In this method, acrylic minirhizotron tubes were transformed into oxygen sensitive planar optodes by applying oxygen-sensitive dyes in a strip along the length of each tube. Successful calibrations of these optodes are presented as proof of concept for this method. The RhizoPi camera system can collect research-quality images of roots and serve as a platform for deploying planar optode technologies for in situ analysis of soil solution chemistry, thus

opening up the possibility of simultaneous collection of soil solution chemistry and root data from the same location.

Introduction

Understanding the relationship between plant roots and belowground processes is essential to agriculture productivity and understanding water, carbon, and nutrient cycles (Richter et al., 1999; Kirkham, 2014). Developing a low-cost, automated tool for imaging and analyzing belowground processes is fundamental for meeting the food demands of a growing human populations. A challenge for belowground analysis is non-destructively collecting data at relevant spatial and temporal scales. Current methods rely on extracting soil samples to quantitatively investigate the physiochemical parameters of the rhizosphere (the volume of soil impacted by surrounding plant roots), thus modifying biogeochemical and physical conditions of significance. Since root development is driven by the biogeochemical conditions within the soil environment, the ability to measure the soil solution chemistry without disturbing the soil and root would represent a significant scientific breakthrough.

Although root imaging with minirhizotron technologies has progressed in ecology, plant ecophysiology, and soil fertility studies (Johnson et al., 2001b; Vamerali et al., 2012b; Iversen et al., 2012), it does not directly contribute to belowground measurements of soil chemistry. To obtain insights on rhizosphere biogeochemistry, minirhizotrons must be paired with technology that facilitates simultaneous soil chemistry data collection. Planar optical sensors (optodes) are a promising technology for quantifying chemical soil solutions. This technology consists of chemically-sensitive dyes embedded in plastic. To date there are dyes sensitive to oxygen, acidity, carbon dioxide, and other dissolved substances (Blossfeld and Gansert, 2012). The dyes, once excited with light at dye-specific wavelengths, fluoresce at intensities that vary with the

target analyte concentration. This fluorescence is then imaged using cameras. Once calibrated, planar optodes facilitate repeatable, two-dimensional analysis of analyte concentrations at the millimeter resolution (Blossfeld and Gansert, 2012).

The coupling of planar optode technologies with an automated minirhizotron camera is an important progression in soil, root, and rhizosphere research. It facilitates in situ analysis of root and fungal hyphae attributes that are paired with soil solution chemistry measurements at the same time and location in the soil. In this chapter I will present a method for coupling the minirhizotron with planar optode. The developed technique is based on the method originally presented by Larsen et al. (2011a).

Material and methods

The oxygen sensitive optode sensor is based on the oxygen-sensitive luminophore, platinum(II) octaethylporphyrin (PtOEP) (Lee and Okura, 1997; Oguri et al., 2006). Platinum (II) octaethylporphyrin is commercially available from Frontier Scientific (frontiersci.com). According to Larsen et al. (2011a), the brightness of the platinum(II) systems can be significantly enhanced by linking the indicator with an antenna dye that operates as an energy contributor for the indicator. The antenna dye efficiently receives the excitation light-energy and shifts the energy to the indicator, which is a principle attributed to light harvesting (Mayr et al., 2009). The principle of light harvesting employs energy transfer (ET) from donor to acceptor dye molecules (Lian et al., 2019). The donor dye serves as antenna for the excitation light and transfers the energy to the analyte sensitive acceptor dye (indicator) (Mayr et al., 2009). In this study, the dye from Macrolex® fluorescence yellow 10GN (MY) was used as the antenna dye,

which is available through LANXESS (lanxess.com). The antenna and indicator dyes present excellent absorption spectra for excitation with commercially-available high power blue LEDs.

A reliable ratio of antenna to indicator dye in this research has been determined to be 1%/1% (wt/wt) in a 4% polystyrene matrix (Larsen et al., 2011a). The antenna dye, indicator dye, and polystyrene were dissolved in toluene to form a solution. In this case, the solution was made with 40 mg of indicator dye, 40 mg of antenna dye, 2 g of polystyrene and 50 g (43 ml) of solvent (Toluene) as described by Waldo et al. (2019) and Turner et al. (2020). This solution was stirred in a beaker until all polystyrene is dissolved over the course of several hours.

Creating Planar Oxygen Optodes with Minirhizotron Tubes

The planar optode dyes were applied to minirhizotron tubes as a spray using an airbrush (model 200, Badger Air-Brush Company, Franklin Park, IL, USA) connected to a small air compressor (6 Gallon Portable Electric Pancake Compressor, Ridge Tool Company, Elyria, OH, USA). Use of the airbrush ensured an even application of the optode dye solution. Minirhizotrons were coated with the dye solution in a fume hood (Figure 3.1), and dye was applied until a consistent orange color was achieved (Figure 3.2). One batch of dye coats approximately two 2.5 cm x 95 cm optodes (approximately 240 cm^2). Once the dye had dried, the sensor was covered with a black, waterproof silicone (black window & door caulk 100%, type II, Momentive Company, Waterford, NY, USA) which functions as an optical insulation to diminish light-scattering artifacts from the soil and roots (Glud et al., 1996). The black silicone is oxygen permeable but does not allow light to be transmitted. This silicone was applied to the optode surface first with a caulk gun, then smoothed by hand with a spatula to a consistent thickness of approximately 1 mm thick.

Modification of the RhizoPi Minirhizotron Camera System for Imaging Planar Optodes

The oxygen-sensitive luminophores are excited by blue light from LEDs as described by Larsen (2011a). The RhizoPi camera uses LEDs (NeoPixel Stick - 8 x 5050 RGB LED with Integrated Drivers, Adafruit industries) that can be set to emit light of different wavelengths and colors, including blue, which was used for imaging the dyes here. Further, cameras specially made without infrared filters are required on DSLR cameras as described by Larsen (2011a). The RhizoPi camera is built using NOIR Raspberry Pi cameras (Raspberry Pi Foundation). Different than Larsen (2011a), no additional filters were placed over the LEDs or over the camera lens for imaging the planar oxygen optodes on the minirhizotron tubes.

Imaging procedures

Images were recorded by the RhizoPi camera five seconds after the LEDs were turned on. We found that a five second exposure time led to an improved response in fluorescence compared to the 0.5-1.5 s exposure time used by Larsen et al. (2011a). Each raw JPG file collected by the camera was transferred by Wi-Fi to a laptop computer and later analyzed. Processing of the stored images was performed using a script (Appendix Code 3.1) written in the Python programming language (Python, version 3.8, Python Software Foundation). That script performs five functions in sequence, including importing modules, importing images in Joint Photographic Experts Group (JPEG) format, standardized cropping of images for analysis, getting data from the images in red, green, and blue (RGB) format, combining the RGB values in the output, and finally plotting the relation between oxygen and pixels.

Calibrating the images

A calibration tank 0.45 m long by 0.2 m wide by 1.1 m tall was constructed using 2.5 cm thick expanded PVC panels (Figure 3.3). The joints were made water-tight by using PVC primer

and glue on each joint, and the joints screwed together. The tank was filled with deionized water. A calibrated dissolved oxygen meter (oxygen sensor) was placed in the center of the tank under water to monitor oxygen concentrations. Compressed nitrogen and oxygen gas was bubbled into the bottom of the tank through aquarium tubing and an aquarium air stone. The regulators on the compressed gas tanks were adjusted to achieve desired dissolved oxygen concentrations based on the readings from the oxygen sensor.

The minirhizotron tubes with planar optodes coated at the external part of the tube were held under the water during this process and were clamped in place to prevent shifting or floating. The optodes were rolled with a foam paint roller to remove any bubbles on the surfaces of the optodes, then were allowed to equilibrate at each oxygen concentration. The optode responds to oxygen concentrations quickly. However, the use of gases to adjust oxygen concentration in the calibration tank results in turbulence and some variability. Thus, it is recommendable to wait at least five minutes to allow the oxygen concentration of the water in the calibration tank to reach a steady state condition before imaging the optode. The cameras were then operated to collect images at each position for the respective oxygen concentrations. The tested oxygen concentrations are presented in Table 3.1, according to the calibrated dissolved oxygen meter (oxygen sensor). A 0% oxygen concentration was achieved using a 20 g/L sodium sulfite solution.

As described per Larsen (2011a), we used the pixel intensity for calibrating the oxygen sensor, the ratio between the intensity of the two green images, and the intensity of the corresponding red image simultaneously recorded by the camera (Eq. 1). The green images are controlled by luminescence from Macrolex yellow coumarin. The luminescence emission controls the red image from the PtOEP. The Macrolex yellow is not quenched by oxygen, and

luminescence intensity is not affected by the oxygen concentration. Thus, the pixel intensity ratio can be calculated as

$$\mathrm{R} = \frac{\mathrm{Red} - \mathrm{Green}}{\mathrm{Green}} \qquad \textbf{Equation 3.1}$$

where R is the pixel intensity ratio, Red the intensity of the red pixels, and Green the pixel intensity of the two green images recorded by the image sensor. There is a possibility that the pixel intensity of red or green can be attributed to the amount of dye applied to a specific portion of the planar optode. However, since the two dyes are mixed prior to application to the optode, the constant green fluorescence functions as an internal reference. Thus, change in red fluorescence can be attributed primarily to responses to dissolved oxygen concentration and not be influence by the amount of dye applied to the optode at that location.

The optode responsiveness is nonlinear with greatest sensitivity at low oxygen rates.

$$\frac{R}{R0} = \left[\alpha + (1-\alpha)\left(\frac{1}{1 + \mathrm{Ksv}\ \cdot \mathrm{C}}\right)\right] \qquad \textbf{Equation 3.2}$$

where α is the unquenchable portion of the luminescence signal, Ksv the Stern-Volmer (Klimant and Wolfbeis, 1995) quenching constant, R the (red-green)/green luminescent intensity ratio, R0 is the ratio in the lack of oxygen, and C the oxygen concentration. Because temperature has a noticeable influence on the oxygen sensor's performance (Borisov et al., 2006), it is essential to implement sensor calibration at the determined temperature. Thus, calibrations were conducted adopting equation 3

$$\mathrm{C} = \frac{R0 - R}{\mathrm{Ksv}\ \cdot (\mathrm{R} - \mathrm{R0}\ \cdot \alpha)} \qquad \textbf{Equation 3.3}$$

Results

Sensor calibration

The calibration for the oxygen planar optode at position two is shown in Figure 3.4, the values are in Table 3.1, and the calibration for the other positions are in Appendix.

A common trend on the calibration curve for the oxygen planar optode is shown in Figure 3.5. The optode's response in terms of pixel intensity is inversely correlated to the oxygen rates (%). In this case, as the oxygen rates increase, more energy absorbed from the blue LED is being quenched by dissolved oxygen resulting in less fluorescence and lower pixel intensity. Red (R) is inversely correlated with the percent oxygen concentration and obtained a value equal to 212.8. In addition, green (G) signal serves as an internal reference and obtained a value of 30.7 as shown in Figure 3.5. Both figures (Figure 3.4 and Figure 3.5) are examples of calibrations performed at each of five positions along the length of the planar optode.

Discussion and Conclusion

The RhizoPi camera coupled with the planar optode approach can be a useful technology for investigating rooting dynamics and other belowground processes that influence soil chemistry, with the added benefit of non-destructively collecting such data at exact location and temporal resolution.

Compared to the color ratiometric planar optode imaging approach proposed by Larsen (2011a), the minirhizotron coupled with planar optodes presents many benefits. Most notably, combining planar optode and minirhizotron technology will facilitate use of planar optodes in field applications. In addition, both root data and soil solution chemistry data can be collected from the same tube at the same time across a range of soil depths with repeated and non-destructive sampling.

This method did require minor modifications to both the RhizoPi camera system and the planar optode method introduced by Larsen et al. (2011). For example, the RhizoPi camera must use a Raspberry Pi NOIR camera rather than a standard Raspberry Pi camera. Also, for the solvent for the dye solution, toluene (Waldo et al., 2019; Turner et al., 2020) was used instead of chloroform proposed by Larsen (2011a). Moreover, the ratio decreases more than 65% when the oxygen concentration increases from 0 to 100% air saturation. Larsen (2011a) obtained a higher ratio (75% decreased from 0-50% of air saturated). We believe that, with similar modifications to the RhizoPi camera system and planar optode methodology, this approach can be adapted to all planar optode sensors that display a dynamic color change as a function of analyte concentration.

In conclusion we note that planar optode sensors are a proven technology. We have shown that, with minor changes to the RhizoPi camera system and planar optode methodology, planar optodes can be coupled with minirhizotrons, thus opening up the possibility of using the planar optode sensors in field applications. Notably, the low-cost and automated function of the RhizoPi minirhizotron camera system will keep the labor and equipment costs for the planar optodes in field settings low. Accessibility will also be improved through open licensing of the software scripts and the RhizoPi camera system design.

References

Blossfeld, S., and D. Gansert. 2012. The Use of Planar Optodes in Root Studies for Quantitative Imaging. Measuring Roots. Springer, Berlin, Heidelberg. p. 83–92

Borisov, S.M., A.S. Vasylevska, Ch. Krause, and O.S. Wolfbeis. 2006. Composite Luminescent Material for Dual Sensing of Oxygen and Temperature. Adv. Funct. Mater. 16(12): 1536–1542. doi: 10.1002/adfm.200500778.

Glud, R., N. Ramsing, J. Gundersen, and I. Klimant. 1996. Planar optrodes: a new tool for fine scale measurements of two-dimensional O2 distribution in benthic communities. Mar. Ecol. Prog. Ser. 140: 217–226. doi: 10.3354/meps140217.

Iversen, C.M., M.T. Murphy, M.F. Allen, J. Childs, D.M. Eissenstat, et al. 2012. Advancing the use of minirhizotrons in wetlands. Plant Soil 352(1–2): 23–39. doi: 10.1007/s11104-011-0953-1.

Johnson, M.G., D.T. Tingey, D.L. Phillips, and M.J. Storm. 2001. Advancing fine root research with minirhizotrons. Environ. Exp. Bot. 45(3): 263–289. doi: 10.1016/S0098-8472(01)00077-6.

Kirkham, M.B. 2014. Principles of soil and plant water relations. Academic Press.

Klimant, I., and O.S. Wolfbeis. 1995. Oxygen-sensitive luminescent materials based on silicone-soluble ruthenium diimine complexes. Anal. Chem. 67(18): 3160–3166.

Larsen, M., S.M. Borisov, B. Grunwald, I. Klimant, and R.N. Glud. 2011. A simple and inexpensive high resolution color ratiometric planar optode imaging approach: application to oxygen and pH sensing. Limnol. Oceanogr. Methods 9(9): 348–360.

Lee, S.-K., and I. Okura. 1997. Porphyrin-doped sol-gel glass as a probe for oxygen sensing. Anal. Chim. Acta 342(2–3): 181–188. doi: 10.1016/S0003-2670(96)00562-4.

Lian, Z., M. Jiang, F. Qiao, Z. Yuan, M.-N. Chen, et al. 2019. Significant enhancement of light-harvesting efficiency through the formation of [2]pseudorotaxane with γ-cyclodextrin based on a bolaamphiphile of salicylaldehyde azine moiety. Dyes Pigments 162: 475–480. doi: 10.1016/j.dyepig.2018.10.062.

Mayr, T., S.M. Borisov, T. Abel, B. Enko, K. Waich, et al. 2009. Light Harvesting as a simple and versatile way to enhance brightness of luminescent sensors. Anal. Chem. 81(15): 6541–6545. doi: 10.1021/ac900662x.

Oguri, K., H. Kitazato, and R.N. Glud. 2006. Platinum octaetylporphyrin based planar optodes combined with an UV-LED excitation light source: An ideal tool for high-resolution O2 imaging in O2 depleted environments. Mar. Chem. 100(1): 95–107. doi: 10.1016/j.marchem.2005.11.005.

Richter, D.D., D. Markewitz, S.E. Trumbore, and C.G. Wells. 1999. Rapid accumulation and turnover of soil carbon in a re-establishing forest. Nature 400(6739): 56–58. doi: 10.1038/21867.

Turner, J.C., C.J. Moorberg, A. Wong, K. Shea, M.P. Waldrop, et al. 2020. Getting to the Root of Plant-Mediated Methane Emissions and Oxidation in a Thermokarst Bog. J. Geophys. Res. Biogeosciences 125(11). doi: 10.1029/2020JG005825.

Vamerali, T., M. Bandiera, and G. Mosca. 2012. Minirhizotrons in Modern Root Studies. Measuring Roots. Springer, Berlin, Heidelberg. p. 341–361

Waldo, N.B., B.K. Hunt, E.C. Fadely, J.J. Moran, and R.B. Neumann. 2019. Plant root exudates increase methane emissions through direct and indirect pathways. Biogeochemistry 145(1–2): 213–234. doi: 10.1007/s10533-019-00600-6.

Figures and Tables

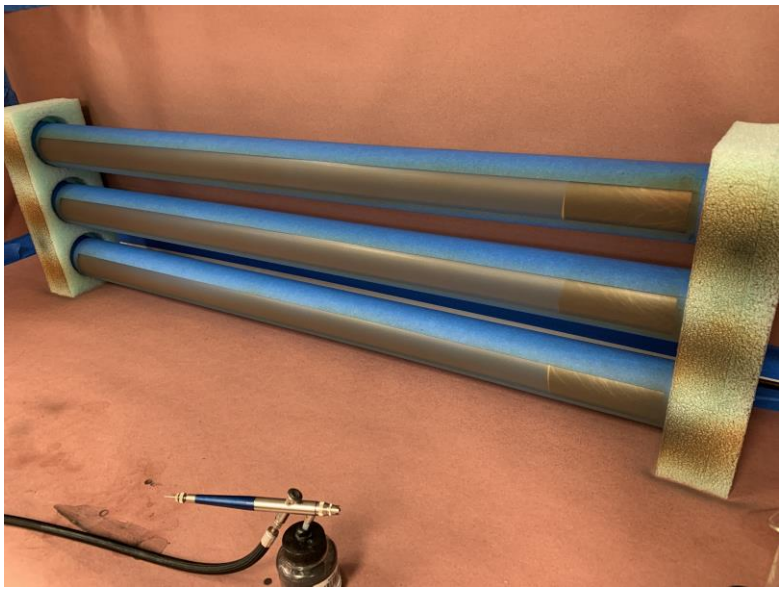

Figure 3.1. Tubes and airbrush into the fume hood for coupling the planar optode.

Figure 3.2. Coding color after painting.

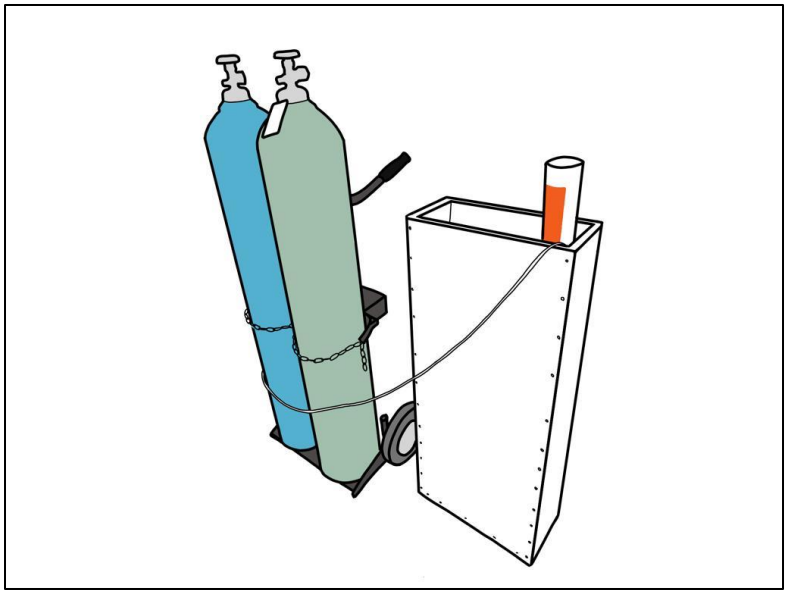

Figure 3.3. Optode calibration tank system.

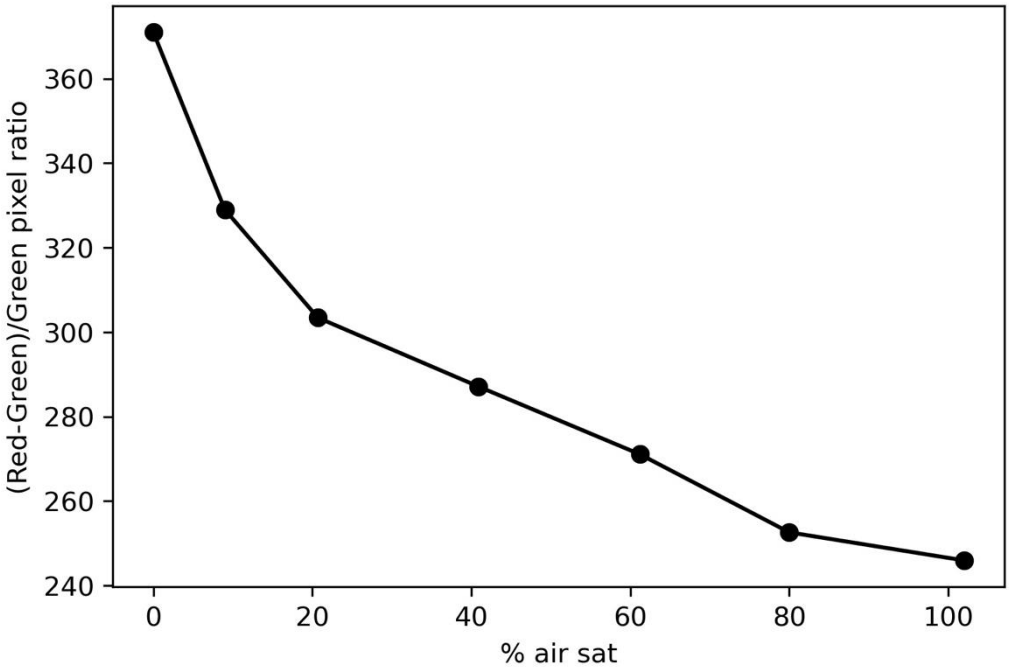

Figure 3.4. An example oxygen optode calibration curve. Dots are mean pixel values for an area of 3 cm^2. This curve is from position 2 of the calibrated optode.

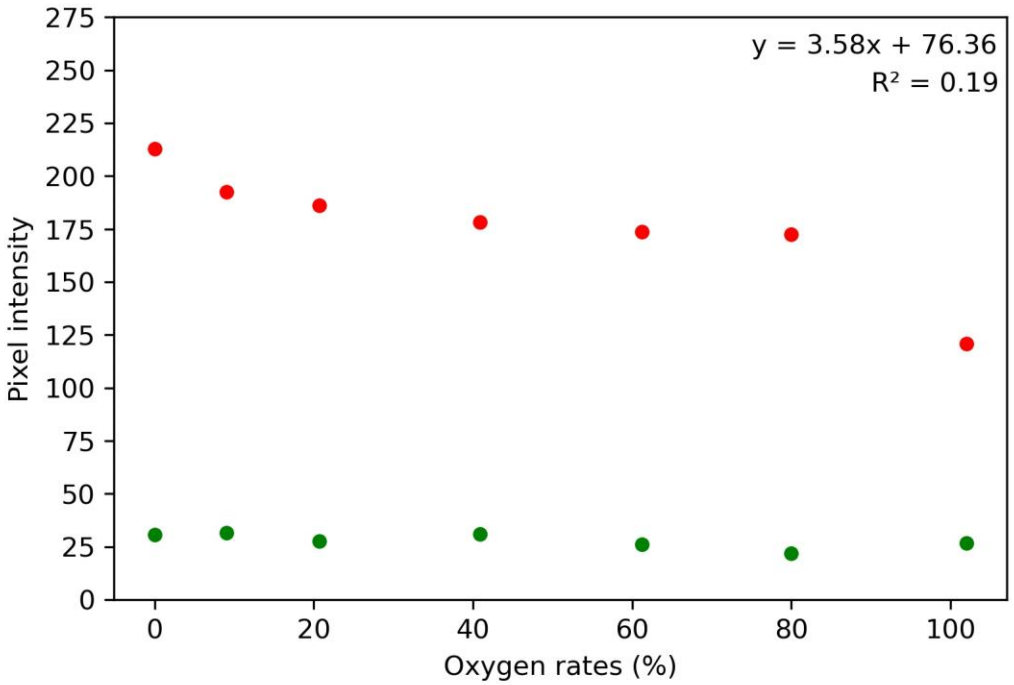

Figure 3.5. Pixel intensity of the Red and Green image at different oxygen concentrations for position 2.

Table 3.1. Oxygen rates, red, green and pixel intensity values for optode calibration of position 2.

Oxygen rates (%)	Red	Green	Pixel intensity
0	212.86	30.7	370.96
9	192.35	31.63	328.96
20.7	186.05	27.65	303.39
40.9	178.09	31.04	287.09
61.2	173.58	26.02	271.06
80	172.37	21.8	252.57
100	120.89	26.61	245.92

Appendix

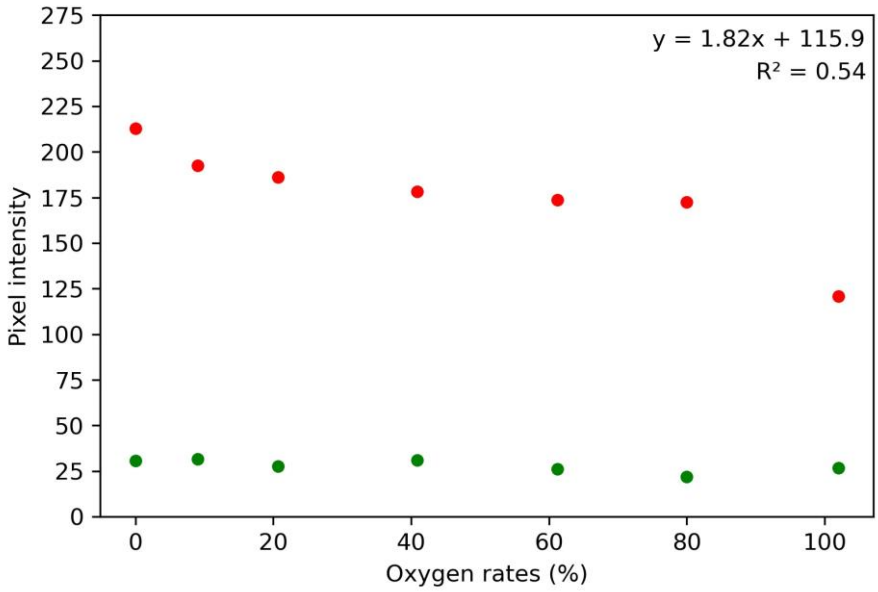

Appendix Figure 3.1. Pixel intensity of the Red and Green image at different oxygen concentrations for position 1.

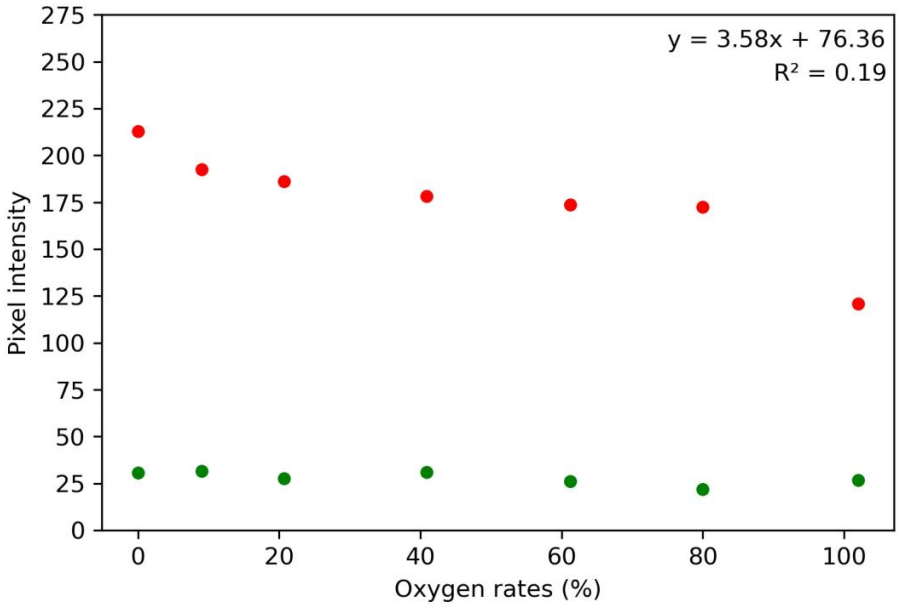

Appendix Figure 3.2. Pixel intensity of the Red and Green image at different oxygen concentrations for position 2.

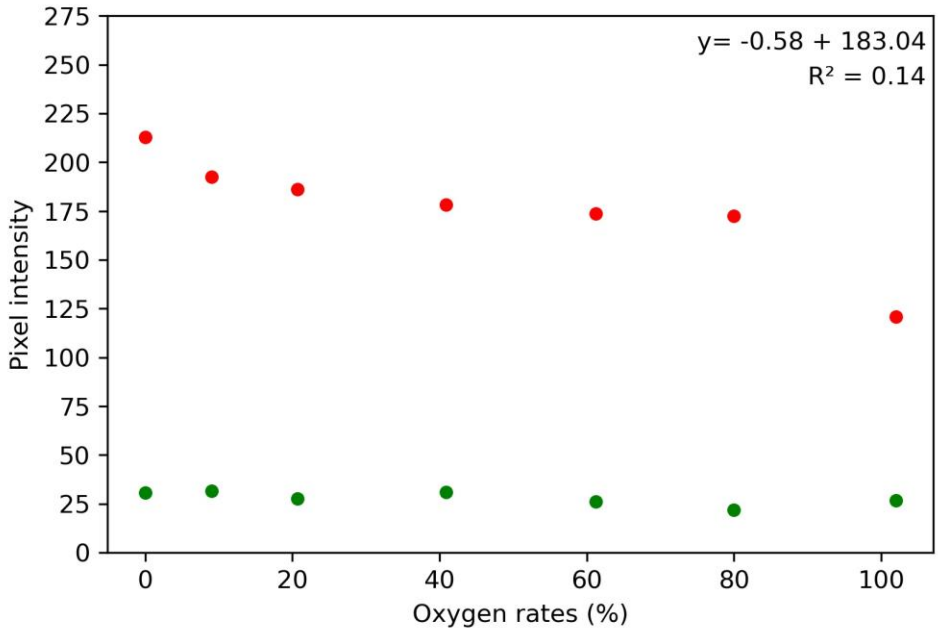

Appendix Figure 3.3. Pixel intensity of the Red and Green image at different oxygen concentrations for position 2.

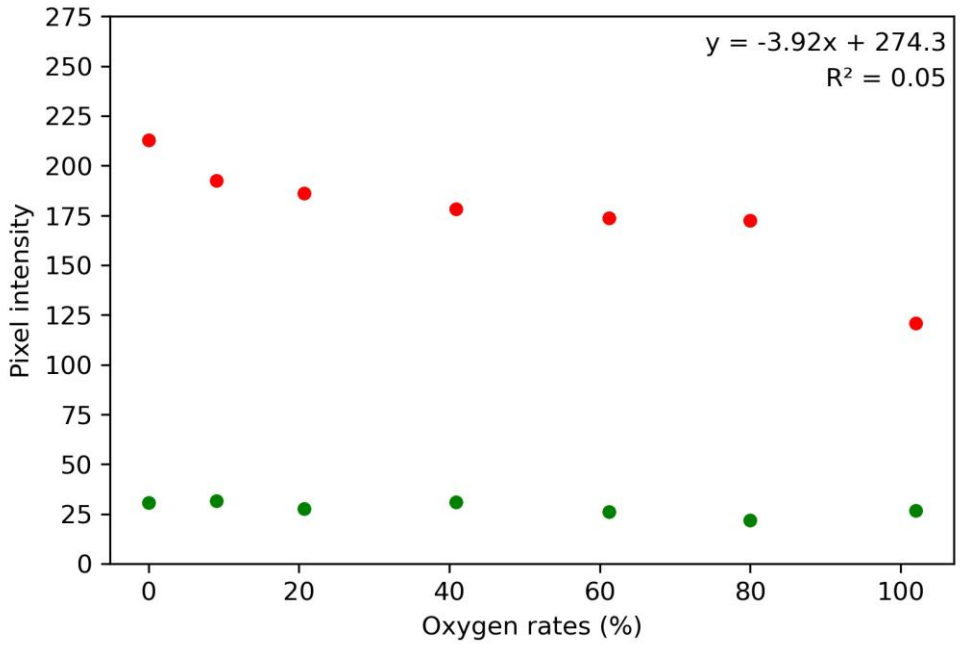

Appendix Figure 3.4. Pixel intensity of the Red and Green image at different oxygen concentrations for position 4.

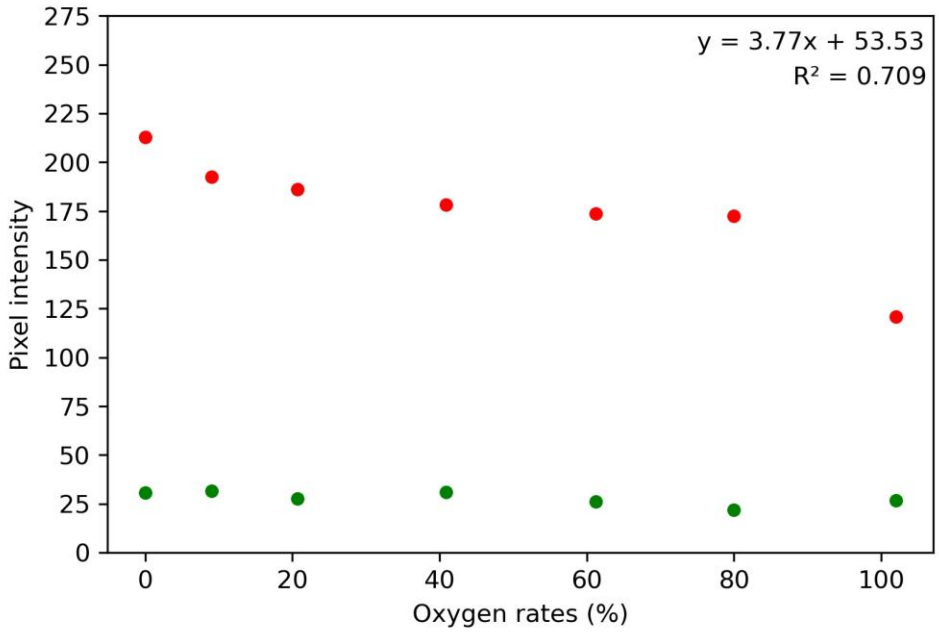

Appendix Figure 3.5. Pixel intensity of the Red and Green image at different oxygen concentrations for position 5.

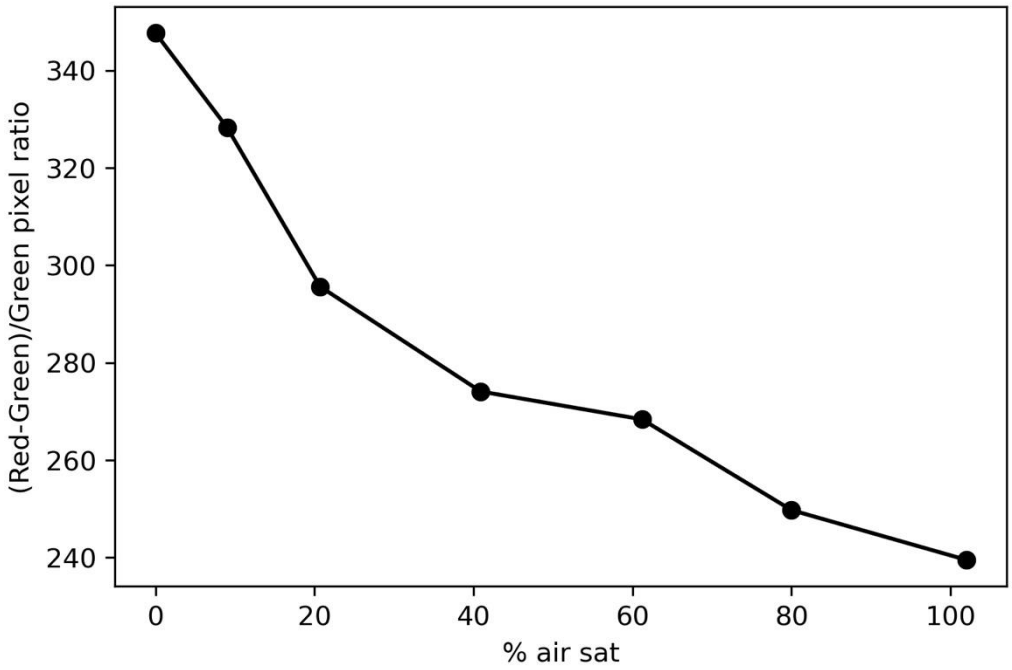

Appendix Figure 3.6. Calibration curve for the oxygen optode in position 1. Dots are mean pixel values for an area of 3 cm^2.

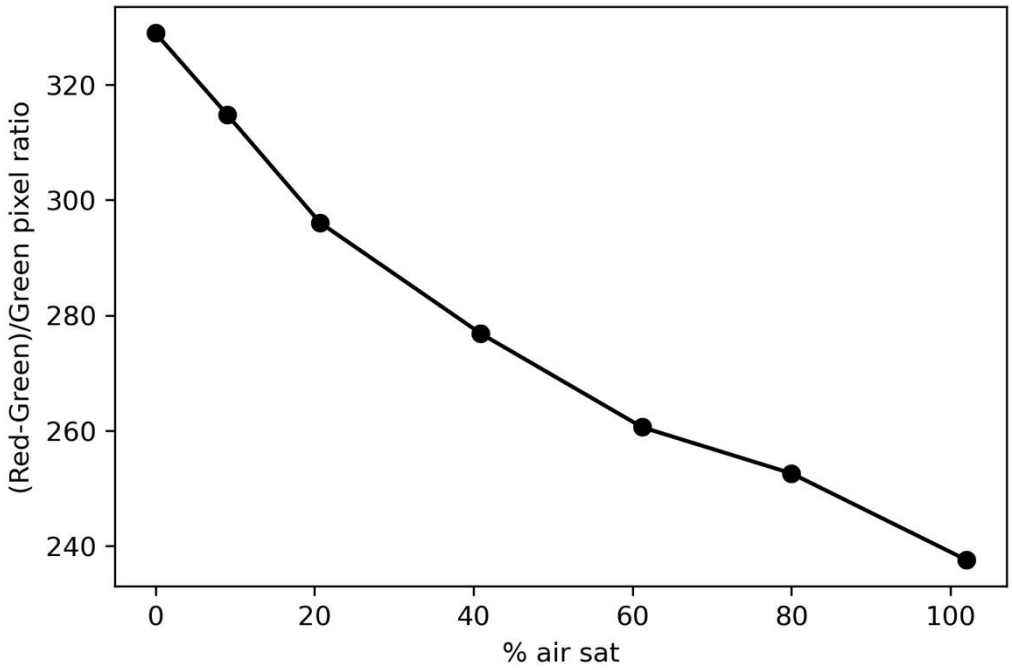

Appendix Figure 3.7. Calibration curve for the oxygen optode in position 3. Dots are mean pixel values for an area of 3 cm^2.

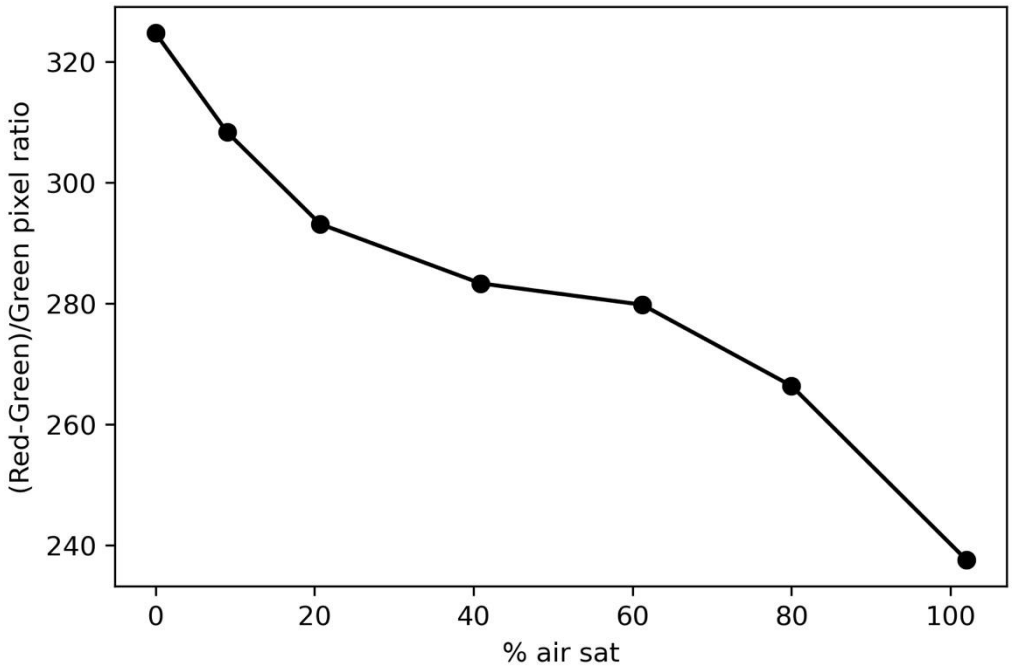

Appendix Figure 3.8. Calibration curve for the oxygen optode in position 4. Dots are mean pixel values for an area of 3 cm^2.

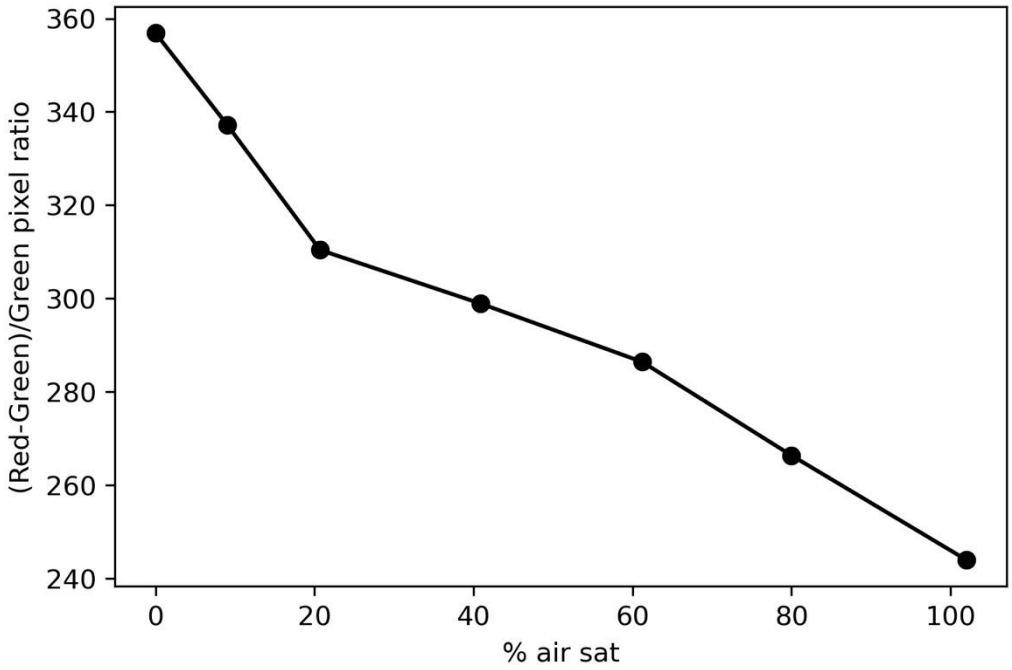

Appendix Figure 3.9. Calibration curve for the oxygen optode in position 5. Dots are mean pixel values for an area of 3 cm^2.

Appendix Table 3.1. Oxygen rates, Red, Green and pixel intensity values for optode calibration of position 1.

Oxygen rates (%)	Red	Green	Pixel intensity
0	205.4	50.2	347.64
9	194.31	43.2	328.27
20.7	186.92	26.71	295.61
40.9	178.7	31.69	274.08
61.2	171.55	27	268.35
80	164.69	25.81	249.73
100	130.19	25.79	239.51

Appendix Table 3.2. Oxygen rates, Red, Green and pixel intensity values for optode calibration of position 3.

Oxygen rates (%)	Red	Green	Pixel intensity
0	200.131	31.81	328.98
9	189.93	25.88	314.85
20.7	185.63	22.46	296.08
40.9	157.76	31.16	276.85
61.2	153	33.96	260.59
80	151.01	20.06	252.57
100	128.97	30.22	237.56

Appendix Table 3.3. Oxygen rates, Red, Green and pixel intensity values for optode calibration of position 4.

Oxygen rates (%)	Red	Green	Pixel intensity
0	212.86	43.85	324.76
9	183.14	21.37	308.37
20.7	180.18	25.58	293.17
40.9	160.31	32.7	283.33
61.2	159.16	30.19	279.81
80	156.57	29.7	266.37
100	125.32	33.4	237.56

Appendix Table 3.4. Oxygen rates, Red, Green and pixel intensity values for optode calibration of position 5.

Oxygen rates (%)	Red	Green	Pixel intensity
0	226.33	43.85	356.88
9	195.51	33.59	337.25
20.7	193.6	30.6	310.4
40.9	185.87	31.16	298.91
61.2	161.53	31.83	286.43
80	159.53	27.61	266.37
100	121.19	26.5	243.98

Appendix Code 3.1. Python code for RGB analysis

```
# Import modules

import numpy as np
import matplotlib.pyplot as plt
import pandas as pd
%matplotlib inline
import cv2
from scipy import stats

# Creating a Data set for each oxygen percentage

images_0 = [cv2.imread(file) for file in
glob.glob("Calibration/T5/0%/*.jpg")]
images_14 = [cv2.imread(file) for file in
glob.glob("Calibration/T5/14.4%/*.jpg")]
images_20 = [cv2.imread(file) for file in
glob.glob("Calibration/T5/20.7%/*.jpg")]
images_40 = [cv2.imread(file) for file in
glob.glob("Calibration/T5/40.9%/*.jpg")]
images_61 = [cv2.imread(file) for file in
glob.glob("Calibration/T5/61.2%/*.jpg")]
images_80 = [cv2.imread(file) for file in
glob.glob("Calibration/T5/80%/*.jpg")]
images_102 = [cv2.imread(file) for file in
glob.glob("Calibration/T5/102%/*.jpg")]
images = [image_0,image_7, image_10, image_15, image_21, image_26, image_31,
image_35,image_41, image_50, image_62, image_79, image_80, image_98]

#Checking the images shape/size
print (image_10.shape)

# Plotting the image file

plt.imshow(image_10)

#Cropping Image
#Create a list of all cropped images from the loop

c=[]
for i in range(0,len(images)):
    cropped_image = images[i][540:740,1080:1280, :] # Select 200x200 in the
middle of the image
    c.append(cropped_image)
    plt.imshow(cropped_image)

# Create variable names and oxygen ratios

images_names = ["image_0",”image_14”, “image_20”, “image_40”, “image_61”,
“image_80”, “image_102]
oxygen_rates = [0, 14.4, 20.7, 40.9, 61.2, 80, 102]
df_mean=pd.DataFrame(columns =
['images','oxygen_rates','red','green','blue','pixel_intensity'])

#index to get folder name
```

```
ind = 0

# For each cropped image, get the images_names, oxygen_rates, and RGB values
to store in a data frame
for crop_image in c:
    #image index
    img = c[ind]

    #oxygen rates
    oxygen = oxygen_rates[ind]

    #image names
    image = images_names[ind]


    # Extract mean data in separate variable for manipulation
    red = crop_image[:, :, 0].mean() #Extract mean of red pixel values
    green = crop_image[:, :, 1].mean() #Extract mean of green pixel values
    blue = crop_image[:, :, 2].mean() #Extract mean of blue pixel values


    #separate values as list, so we can append it!
    #values = [image_names,oxygen_rates,red,green,blue]
    df_mean = df_mean.append({'images':image, 'red':red,
                              "green":green,'blue':blue,
'oxygen_rates':oxygen},ignore_index=True)


    #add index, to get the proper folder name!
    ind = ind + 1

#Create the variable Pixel intensity - Sum of RGB
df_mean["pixel_intensity"]= df_mean[["red", "green",
"blue"]].sum(axis='columns')

#Rounding the Data Frame values
df_mean.round(decimals=2)

# Plotting histograms to analize the rgb data in single bands
plt.figure(figsize=(12,8))

plt.subplot(1,3,1)
plt.hist(df_mean['red'],color= 'r')
plt.xlabel("Red", size=13) # Adding axis x label for red band and its size
plt.yticks([0.5,1,1.5,2,2.5]) # Adjusting the y axis scale for red band

plt.subplot(1,3,2)
plt.hist(df_mean['green'],color= 'g')
plt.xlabel("Green", size=13) # Adding axis x label for green band and its
size
plt.yticks([0.5,1,1.5,2,2.5]) # Adjusting the y axis scale for green band

plt.subplot(1,3,3)
plt.hist(df_mean['blue'],color= 'b')
plt.xlabel("Blue", size=13) # Adding axis x label for blue band and its size
plt.yticks([0.5,1,1.5,2,2.5]) # Adjusting the y axis scale for blue band
```

```
# Compare Oxygen and Pixel intensity with

x = np.array(df_mean["pixel_intensity"]) #Generate data
y = np.array(df_mean["oxygen_rates"])
plt.plot(x, y, 'o') #Create scatter plot
m, b=np.polyfit(x, y, 1) # Adding line that best fits
plt.plot(x, m*x + b, color='b') # m =slope, b =intercept

# Adjusting graph

plt.plot(color=blue) # Plotting the graph
plt.xlabel('Pixel intensity(px)') # Defining the axis (x,y)
plt.ylabel('Oxygen(%)')
plt.title("Oxygen x Pixel Intensity") # Adding title
plt.savefig("../Output/Project-Image.png") # Output - Save the graph to .png
object

# Fit linear model using linregress

df_mean[["oxygen_rates"]] = df_mean[["oxygen_rates"]].apply(pd.to_numeric)
x= df_mean["pixel_intensity"]
y= df_mean["oxygen_rates"]
fit_info = stats.linregress(x, y)

# Display individual parameters

print('slope:',fit_info.slope)
print('intercept:',fit_info.intercept)
print('r:',fit_info.rvalue)
print('r-squared:',fit_info.rvalue**2)
print('p-value:',fit_info.pvalue)

# Output - Save dataframe to .csv object

df_mean.to_csv("../Output/df_Project-Image.csv")
```